

<sup>1</sup> **GLO-Roots: an imaging platform enabling multidimensional characterization of soil-grown root systems**

<sup>3</sup> Rubén Rellán-Álvarez<sup>1, 9</sup>, Guillaume Lobet<sup>2</sup>, Heike Lindner<sup>1, 8</sup>, Pierre-Luc Pradier<sup>1, 8, 10</sup>,  
<sup>4</sup> Jose Sebastian<sup>1, 8</sup>, Muh-Ching Yee<sup>1</sup>, Yu Geng<sup>1, 7</sup>, Charlotte Trontin<sup>1</sup>, Therese LaRue<sup>3</sup>,  
<sup>5</sup> Amanda Schrager-Lavelle<sup>4</sup>, Cara H. Haney<sup>5</sup>, Rita Nieu<sup>6</sup>, Julin Maloof<sup>4</sup>, John P. Vogel<sup>7</sup>,  
<sup>6</sup> José R. Dinneny<sup>1, 12</sup>

<sup>7</sup> <sup>1</sup> Department of Plant Biology, Carnegie Institution for Science, Stanford, CA, USA.

<sup>8</sup> <sup>2</sup> PhytoSystems, University of Liège, Liège, Belgium.

<sup>9</sup> <sup>3</sup> Department of Biology, Stanford University, Stanford, CA, USA.

<sup>10</sup> <sup>4</sup> Department of Plant Biology, UC Davis, Davis, CA, USA.

<sup>11</sup> <sup>5</sup> Harvard Medical School, Massachusetts General Hospital, Department of Genetics, De-  
<sup>12</sup> partment of Molecular Biology Boston, MA, USA

<sup>13</sup> <sup>6</sup> USDA Western Regional Research Center, Albany, CA, USA

<sup>14</sup> <sup>7</sup> DOE Joint Genome Institute, Walnut Creek, CA, USA

<sup>15</sup> <sup>8</sup> These authors contributed equally

<sup>16</sup> <sup>9</sup> Present address: Laboratorio Nacional de Genómica para la Biodiversidad (Langebio),  
<sup>17</sup> Unidad de Genómica Avanzada, Centro de Investigación y de Estudios Avanzados del Insti-  
<sup>18</sup> tuto Politécnico Nacional (CINVESTAV-IPN), Irapuato, Guanajuato, México

<sup>19</sup> <sup>10</sup> Present address: Boyce Thompson Institute for Plant Research/USDA, Ithaca, NY, USA.

<sup>20</sup> <sup>11</sup> Present address: Energy Biosciences Institute, UC, Berkeley, CA, USA

<sup>21</sup> <sup>12</sup> Corresponding author

<sup>22</sup> **Author contributions:**

<sup>23</sup> RR-A: Conception, design and development of the growth and imaging system and Arabidop-  
<sup>24</sup> sis transgenic lines; acquisition, analysis and interpretation of data; drafting and revising

25 the article.

26 GL: Development of the GLO-RIA image analysis plugin, analysis and interpretation of

27 data, drafting and revising the article.

28 HL: Acquisition of data, development of the tomato growth and imaging setup.

29 P-LP: Acquisition of data, analysis and interpretation of data

30 JS: Development of Brachypodium transgenic lines, acquisition and analysis of Brachy-

31 podium, Arabidopsis and tomato data.

32 MCY: Development of Arabidopsis and Brachypodium transgenic lines.

33 YG: Development of Arabidopsis transgenic lines.

34 CT: Acquisition and analysis of the QPCR data

35 TL: Acquisition and analysis of the QPCR data

36 AS-L: Contributed the unpublished dual-color tomato line.

37 CH: Contributed the unpublished *Pseudomonas fluorescens* CH267-lux strain.

38 RN: Contribution to the development of the Brachypodium transgenic line.

39 JM: Contributed the unpublished dual-color tomato line.

40 JPV: Contribution to the development of the Brachypodium transgenic line.

41 JRD: Conception, design and development of the growth and imaging system and Arabidop-

42 sis transgenic lines; acquisition, analysis and interpretation of data; drafting and revising

43 the article.

44 All authors read and approve the final version of the manuscript.

45 **Abstract**

46 Root systems develop different root types that individually sense cues from their local

47 environment and integrate this information with systemic signals. This complex multi-

48 dimensional amalgam of inputs enables continuous adjustment of root growth rates, direc-  
49 tion and metabolic activity that define a dynamic physical network. Current methods for  
50 analyzing root biology balance physiological relevance with imaging capability. To bridge  
51 this divide, we developed an integrated imaging system called Growth and Luminescence  
52 Observatory for Roots (GLO-Roots) that uses luminescence-based reporters to enable stud-  
53 ies of root architecture and gene expression patterns in soil-grown, light-shielded roots. We  
54 have developed image analysis algorithms that allow the spatial integration of soil properties,  
55 gene expression and root system architecture traits. We propose GLO-Roots as a system  
56 that has great utility in presenting environmental stimuli to roots in ways that evoke natural  
57 adaptive responses and in providing tools for studying the multi-dimensional nature of such  
58 processes.

## 59 **Introduction**

60 Plant roots are three-dimensional assemblies of cells that coordinately monitor and acclimate  
61 to soil environmental change by altering physiological and developmental processes through  
62 cell-type and organ-specific regulatory mechanisms<sup>1,2</sup>. Soil comprises a complex distribution  
63 of particles of different size, composition and physical properties, airspaces, variation in  
64 nutrient availability and microbial diversity<sup>3,4</sup>. These physical, chemical and biological  
65 properties of soil can vary on spatial scales of meters to microns, and on temporal scales  
66 ranging from seasonal change to seconds. Root tips monitor this environment through  
67 locally and systemically acting sensory mechanisms<sup>5,6</sup>.

68 The architecture of the root system determines the volume of soil where resources can be  
69 accessed by the plant (rhizosphere) and is under both environmental and genetic control.  
70 Plasticity in growth parameters allows the plant to adjust its form to suit a particular soil.  
71 Lateral roots, which usually make up the majority of the total root system, often grow at an  
72 angle divergent from the gravity vector. This gravity set-point angle (GSA) is controlled by  
73 auxin biosynthesis and signaling and can be regulated by developmental age and root type<sup>7</sup>.  
74 Recent cloning of the *DRO1* Quantitative Trait Locus (QTL) demonstrates that natural

75 genetic variation is a powerful tool for uncovering such control mechanisms<sup>8</sup>.

76 Specific root ideotypes (idealized phenotypes) have been proposed to be optimal for acquisi-  
77 tion of water and nitrogen, which are distinct from ideotypes for low phosphorus. Based on  
78 computational modeling and field studies, the “steep, deep and cheap” ideotype proposed by  
79 Lynch and colleagues may provide advantages to the plant for capturing water and elements  
80 like nitrogen that are water soluble and therefore tend to move in the soil column with water.  
81 This ideotype consists of highly gravitropic, vertically oriented roots that grow deep in the  
82 soil column and develop large amounts of aerenchyma, which reduces the overall metabolic  
83 cost of the root system<sup>3</sup>. Other nutrients, like phosphorus, which have limited water solu-  
84 bility and are tightly bound to organic matter, usually accumulate in the top layers of soil  
85 and favor root systems that are more highly branched and shallow. The low-phosphorus  
86 ideotype effectively increases root exploration at the top layers of soil<sup>3</sup>. Modeling of root  
87 system variables shows that optimum architecture for nitrogen and phosphorus uptake are  
88 not the same<sup>9</sup> and suggests tradeoffs that may affect the evolution of root architecture as a  
89 population adapts to a particular environmental niche<sup>10</sup>.

90 Clearly, understanding the architecture of root systems and how environmental conditions  
91 alter root developmental programs is important for understanding adaptive mechanisms of  
92 plants and for identifying the molecular-genetic basis for different response programs. In  
93 addition, root systems have complexity beyond their architecture that needs to be incorpo-  
94 rated into our understanding of plant-environment interactions. Primary and lateral roots  
95 exhibit different stress response programs in *Arabidopsis*<sup>2,11</sup> and may play specialized roles  
96 in water and nutrient uptake. Thus, it is important to develop methods that allow for a  
97 multidimensional characterization of the root system that includes growth, signaling, and  
98 interactions with other organisms. Furthermore, physiological parameters that affect whole  
99 plant responses to the environment, such as transpiration, are likely integrated into such  
100 processes, thus requiring a more holistic approach to studies of root function.

101 Based on these considerations we have developed a new root imaging platform, Growth  
102 and Luminescence Observatory for Roots (GLO-Roots), which allows root architecture and

103 gene expression to be studied in soil-grown plants. GLO-Roots is an integrated system  
104 composed of custom growth vessels, luminescent reporters and imaging systems. We use  
105 rhizotrons that have soil volumes equivalent to small pots and support growth of Arabidopsis  
106 from germination to senescence. To visualize roots, we designed plant-codon optimized  
107 luciferase reporters that emit light of different wavelengths. To visualize reporter expression,  
108 plants are watered with a dilute luciferin solution and imaged afterwards. We have built  
109 a custom luminescence imaging system that automatically captures images of rhizotrons  
110 held vertically. The signal from each reporter is distinguished using band-pass filters held  
111 in a motorized filter wheel, which enables automated acquisition of images from plants  
112 expressing both structural and environmentally and developmentally responsive reporters.  
113 We have also developed GLO-RIA (GLO-Roots Image Analysis), an ImageJ<sup>12</sup> plugin that  
114 allows for automated determination of (among other traits) root system area, convex hull,  
115 depth, width and directionality, which quantifies the angle of root segments with respect  
116 to gravity. GLO-RIA is also able to relate root system parameters to local root-associated  
117 variables such as reporter expression intensity and soil-moisture content.

118 Overall GLO-Roots has great utility in presenting environmental stimuli to roots in phys-  
119 iologically relevant ways and provides tools for characterizing responses to such stimuli at  
120 the molecular level in whole adult root systems over broad time scales.

121 **Box 1.**

122 All resources for GLO-Roots, including the original raw data used in the manuscript, sample  
123 images, GLO-RIA user manual, the latest software updates and the source code, can be  
124 found at: <https://dinnenylab.wordpress.com/glo-roots/>

125 **Results.**

126 We have developed an integrated platform for growing, imaging and analyzing root growth  
127 that provides advances in physiological relevance and retains the ability to visualize aspects

<sup>128</sup> of root biology beyond structure.

<sup>129</sup> **The GLO-Roots platform.**

<sup>130</sup> GLO-Roots is comprised of four parts: i) growth vessels called rhizotrons that allow plant  
<sup>131</sup> growth in soil and root imaging; ii) luminescent reporters that allow various aspects of root  
<sup>132</sup> biology to be tracked in living plants; iii) GLO1 luminescence-imaging system designed to  
<sup>133</sup> automatically image rhizotrons; iv) GLO-RIA, an image analysis suite designed to quantify  
<sup>134</sup> root systems imaged using GLO-Roots.

<sup>135</sup> **Plant growth system.** GLO-Roots utilizes custom designed growth vessels classically  
<sup>136</sup> known as rhizotrons, which hold a thin volume of soil between two sheets of polycarbonate  
<sup>137</sup> plastic. Acrylic spacers provide a 2-mm space in which standard peat-based potting mix  
<sup>138</sup> is added. Black vinyl sheets protect roots from light and rubber U-channels clamp the rhi-  
<sup>139</sup> zotron materials together. Plastic racks hold the rhizotrons vertically and further protect  
<sup>140</sup> the roots from light. Rhizotrons and rack are placed in a black tub and water is added, to  
<sup>141</sup> a depth of about 2 cm, at the bottom to maintain moisture in the rhizotrons during plant  
<sup>142</sup> growth. The volume of soil in the rhizotrons ( $100 \text{ cm}^3$ ) is similar to small pots commonly  
<sup>143</sup> used for *Arabidopsis* and supports growth throughout the entire life cycle (Fig 1A-C and  
<sup>144</sup> Supplement 1).

<sup>145</sup> To determine how the biology of plants grown in rhizotrons compares to other standard  
<sup>146</sup> growth systems, we utilized high-throughput qRT-PCR to study how these conditions af-  
<sup>147</sup> fect expression of 77 marker genes in root and shoot samples. These genes were curated  
<sup>148</sup> from the literature and belong to a wide array of biological pathways including nutrient  
<sup>149</sup> acquisition, hormone and light response and abiotic stress. Whole roots and shoot samples  
<sup>150</sup> were collected at the end of the light and dark periods (Long-day conditions: 16 hour light,  
<sup>151</sup> 8 hours dark) from plants grown in rhizotrons, pots, and petri dishes with two different  
<sup>152</sup> media compositions: 1X Murashige and Skoog basal salts (ms) 1% sucrose or 0.25X ms,  
<sup>153</sup> no sucrose (ms25). Principal component analysis of the gene expression values showed a  
<sup>154</sup> separation of soil and gel-grown root systems in the the first principal components (Figure

155 1-figure supplement 1A). In roots grown on gel-based media, we observed enhanced expres-  
156 sion of genes associated with light-regulated pathways (flavonoid biosynthesis: *FLAVINOL*  
157 *SYNTHASE1*, *FLS1*, *CHALCONE SYNTHASE*, *CHS* and photosynthesis: *RUBISCO SUB-*  
158 *UNIT 1A*, *RBCS1A*, *CYCLOPHILIN 38*, *CYP38*), which is expected due to the exposure  
159 of gel-grown roots to light. In addition, genes associated with phosphorus nutrition (*LOW*  
160 *PHOSPHATE RESPONSE1*, *LPR1*, *PHOSPHATE STARVATION RESPONSE1*, *PHR1*)  
161 were (Figure 1-figure table supplement 1) less expressed in soil-grown roots, suggesting dif-  
162 ferences in nutrient availability between the different growth systems. Interestingly, shoot  
163 samples where not as clearly separated by growth media and, instead, time of day had a  
164 greater effect (Figure 1-Supplement 2). These data suggest root systems may be partic-  
165 ularly sensitive to media conditions and indicate that rhizotron-grown root systems more  
166 closely approximate the biology of pot-grown plants than standard gel-based media. Shoot  
167 weight and primary root length were significantly reduced for gel-grown plants compared  
168 to rhizotron- or pot-grown plants suggesting significant differences in the biology of plants  
169 grown under these conditions (Figure 1-figure supplement 1B-C).

170 While the 2 mm depth of the soil sheet is 10 to 20 times the average diameter of an Arabidop-  
171 sis root (between 100-200 microns<sup>13</sup>), we evaluated whether rhizotron-grown plants exhibited  
172 any obvious stress as a consequence of physical constriction. We compared traits of plants  
173 growing in vessels that hold similar volumes of soil but in different volumetric shapes. The  
174 number of lateral roots was significantly lower in pot and cylinder-grown plants compared  
175 to rhizotron-grown plants (Figure 1-figure supplement 1D) whereas primary root length of  
176 rhizotron and cylinder-grown plants was significantly greater than pot-grown plants (Figure  
177 1-figure supplement 1E). No significant differences in shoot area were observed between the  
178 three systems (Figure 1-figure supplement 1-data). Thus, these data do not support the  
179 hypothesis that rhizotron-grown plants experience physical constriction greater than other  
180 vessels holding the same volume of soil.

181 **Generation of transgenic plants expressing different luciferases.** Arabidopsis roots  
182 cannot easily be distinguished from soil using brightfield imaging due to their thinness and

183 translucency (Figure 1-figure supplement 3); thus, reporter genes are needed to enhance the  
184 contrast between the root and their environment. Luciferase is an ideal reporter to visualize  
185 roots: 1) unlike fluorescent reporters, luciferase does not require high-intensity excitation  
186 light, which could influence root growth, 2) peat-based soil (a type of histosol) exhibits no  
187 autoluminescence but does autofluoresce at certain excitation wavelengths similar to GFP  
188 (Figure 1-figure supplement 3), 3) while GFP is very stable, and thus not as suitable for  
189 imaging dynamic transcriptional events, the luciferase enzyme is inactivated after catabolism  
190 of luciferin, making it ideal for studying processes such as environmental responses. A  
191 considerable number of luciferases have been developed that emit light spanning different  
192 regions of the visible spectrum, but their utilization has been limited to studies in animals  
193 (Table 1).

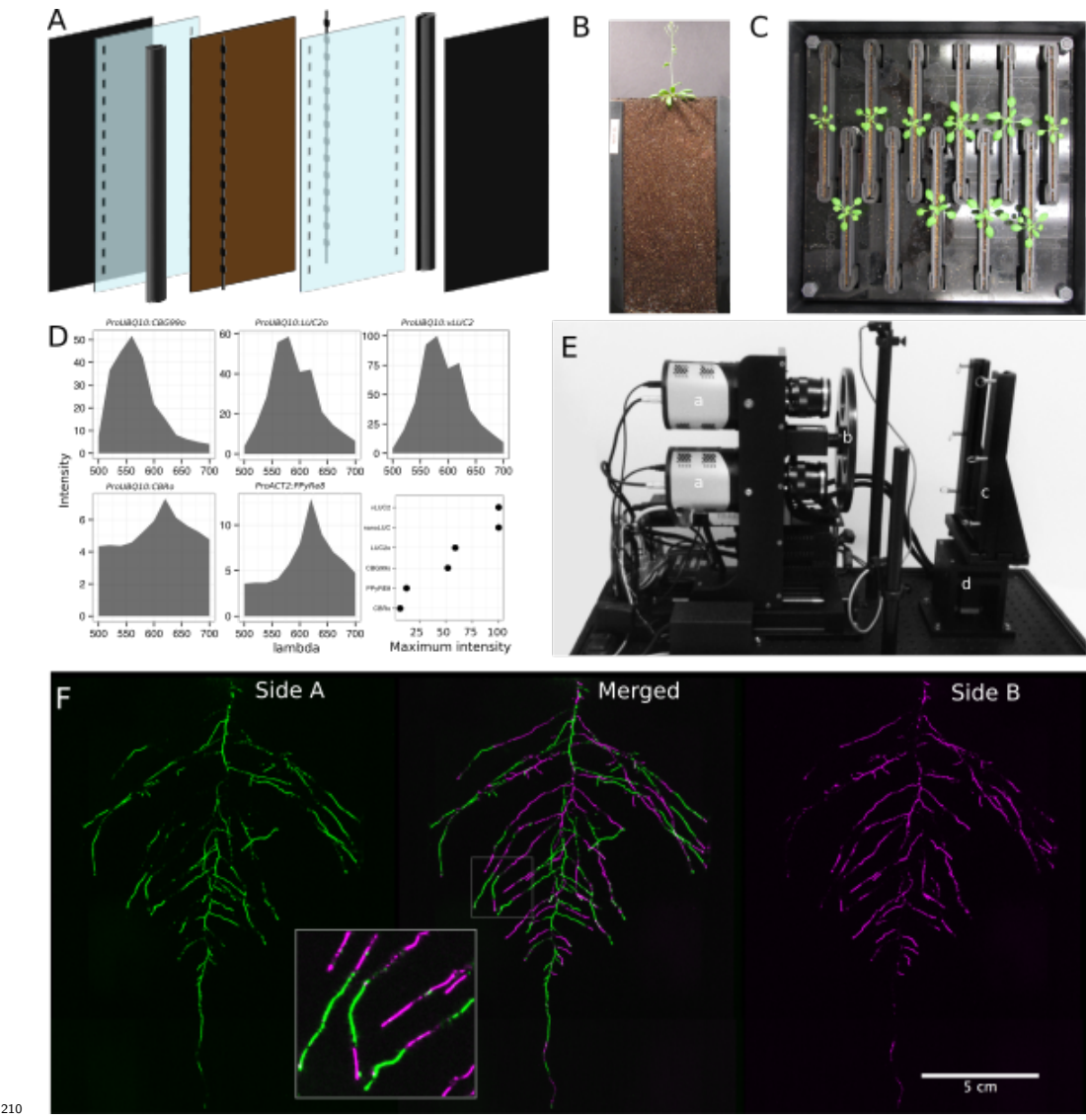
194 **Table 1:** Luciferases used in this study.

Luciferase	Origin	maximum wavelength	Substrate
Ppy RE8	firefly	618	D-luciferin
CBGRed	click beetle	615	D-luciferin
venus-LUC2	FP + firefly	580	D-luciferin
LUC(+)	firefly	578	D-luciferin
CBG99	click beetle	537	D-luciferin
lux operon	A. fischeri	490	biosynthesis pathway encoded within operon
nanoLUC	Deep sea shrimp	470	furimazine

195 To determine the efficacy of using luciferase to visualize roots in soil, we codon optimized  
196 sequences of *PpyRE8*, *CBGRed*, *LUC2*, and *CBG99* for Arabidopsis expression. In addition,  
197 nanoLUC<sup>14</sup> and venus-LUC2<sup>15</sup> were utilized. Constitutive luciferase expression was driven  
198 in plants using the *UBIQUITIN 10 (UBQ10)* or *ACTIN2 (ACT2)* promoters using vectors  
199 assembled through a Golden-Gate cloning system<sup>16</sup>. Plants homozygous for a single locus  
200 T-DNA insertion were evaluated for in vivo emission spectra and luminescence intensity  
201 (Fig 1D). All the evaluated luciferases use D-luciferin as a substrate facilitating the simulta-

<sup>202</sup> neous imaging of different luciferases except nanoLUC, which uses a proprietary substrate  
<sup>203</sup> furimazine<sup>14</sup>. Luciferases with red-shifted emission spectra were less intense than the green-  
<sup>204</sup> shifted luciferases (Fig 1D). LUC2o showed an emission maximum at 580 nm and a minor  
<sup>205</sup> peak at 620 nm while CBG99o lacks the minor peak.

<sup>206</sup> Continuous addition of luciferin did not have any significant effect on shoot weight or primary  
<sup>207</sup> root length (Figure 1-figure supplement 4). After luciferin addition, luminescence signal  
<sup>208</sup> could be reliably detected in root systems for up to 10 days, depending on the developmental  
<sup>209</sup> state of the plant.



211 **Figure 1. GLO-Roots growth and imaging systems** A) 3D representation of the  
 212 different physical components of the rhizotron: plastic covers, polycarbonate sheets, spacers  
 213 and rubber U-channels. Blueprints are provided in Supplementary material 1. In brown,  
 214 soil layer. B) Thirty five day-old plant in rhizotron with black covers removed. C) Top view  
 215 of holding box with eleven rhizotrons. D)In vivo emission spectra of different luciferases  
 216 used in this study. Transgenic homozygous lines expressing the indicated transgenes were  
 217 grown on agar media for 8 days. Luciferin (300  $\mu$ M) was sprayed on the seedlings and

218 plates were kept in the dark and then imaged for 2 s at wavelengths ranging from 500  
219 to 700 nm. Five intensity values were taken from different parts of the roots of different  
220 seedlings and averaged. Relative maximum intensity values are indicated in the lower right  
221 graph. E) GLO 1 imaging system. The system is composed by two back illuminated CCD  
222 cameras (a) cooled down to -55 °C. A filter wheel (b) allows for spectral separation of the  
223 different luciferases. On the right, a rhizotron holder (c) is used to position the rhizotrons  
224 in front of the cameras. A stepper motor (d) rotates the rhizotron 180° to image both  
225 sides. F) A 21 DAS plant expressing *ProUBQ10:LUC2o* was imaged on each of two sides  
226 of the rhizotron; luminescence signal is colorized in green or magenta to indicate side. In  
227 the middle of the panel, a combined image of the two sides is shown. The inset shows a  
228 magnified part of the root system. FW: fresh weight, PR: Primary root.

229 **GLO1: a semi-automated luminescence imaging system for rhizotrons.** Lumines-  
230 cence imaging systems commercially available for biomedical research are usually optimized  
231 for imaging horizontally held specimens or samples in microtiter plates. Placing rhizotrons  
232 in this position would induce a gravitropic response in plants. Working with Bioimaging So-  
233 lutions (San Diego, CA) we designed and built a luminescence imaging system optimized for  
234 rhizotron-grown plants. GLO1 (Growth and Luminescence Observatory 1) uses two PIXIS-  
235 XB back-thinned CCD cameras (Princeton Instruments, Trenton, NJ, USA) to capture  
236 partially-overlapping images of rhizotrons while a motorized stage automatically rotates the  
237 rhizotron to capture images of both sides (Fig 1E). A composite image is generated from  
238 the images captured of each side; Fig 1F shows that approximately half of the root sys-  
239 tem is revealed on each side with few roots being visible on both sides. Apparently, the  
240 soil sheet is thick enough to block portions of the root system but thin enough to ensure  
241 its continuous structure can be compiled from opposite face views. We tested the ability  
242 of GLO1-generated images to reveal complete root systems by manually quantifying the  
243 number of lateral roots in excavated root systems of 8 different plants and testing these  
244 results against estimates of lateral root number from images of the same plants visually in-  
245 spected by 4 different persons. These comparisons revealed good correlation ( $(R^2 = 0.974)$ )

246 between actual lateral root counts and image-based estimation, indicating GLO1-generated  
247 root images provide an accurate representation of the in soil root system.

248 **GLO-RIA: GLO-Roots Image Analysis.** We developed a set of image analysis algo-  
249 rithms that were well suited for the complex root systems that GLO-Roots is able to capture.  
250 GLO-RIA (Growth and Luminescence Observatory Root Image Analysis) is an ImageJ plu-  
251 gin divided in two modules.

252 The first module (RootSystem) performs four different types of analysis: i) a local analysis  
253 that detects all root particles in the image and computes their position, length and direction;  
254 ii) the global analysis performs a root system level analysis and computes the total visible  
255 surface, convex hull, width and depth; iii) the shape analysis uses Elliptic Fourier Descrip-  
256 tors or pseudo-landmarks similarly to RootScape<sup>17</sup> to perform a shape analysis on the root  
257 system iv) the directionality analysis computes the mean direction of root particles in a  
258 root system (either on the full image or by a user-defined region of interest in the image).  
259 These four analysis methods are fully automated by default, but can be manually adjusted  
260 if needed.

261 The second module of GLO-RIA (RootReporter) was specifically designed for the analysis of  
262 multi-layered images such as combinations of gene reporter, root structure and soil moisture.  
263 Shortly, the plugin works as follows: i) detection of the gene reporters and the structure  
264 reporters in their respective images; ii) if needed, a manual correction can be performed to  
265 correct the automated detection; iii) gene reporters are linked with the soil water content  
266 and the structure reporters, based on their proximity; iv) gene reporter intensity (either  
267 absolute or normalized using the structural reporter) is computed; v) all data are exported  
268 and saved to a Root System Markup Language (RSML) datafile<sup>18</sup>. Gene and structure  
269 reporters can be followed across different time and space points. Using an object oriented  
270 approach, great care has been taken to facilitate the user interactions on the different images  
271 to streamline the analysis process. Table 2 shows a list of root system features extracted  
272 using GLO-RIA.

273 **Table 2:** list of root system features extracted using GLO-RIA.

variable	unit
projected area	cm <sup>2</sup>
number of visible roots	-
depth	cm
width	cm
convex hull area	cm <sup>2</sup>
width	cm
feret	cm
feret angle	°
circularity	-
roundness	-
solidity	-
center of mass	cm
Directionality	°
Euclidean Fourier Descriptors	-
Pseudo landmarks	-

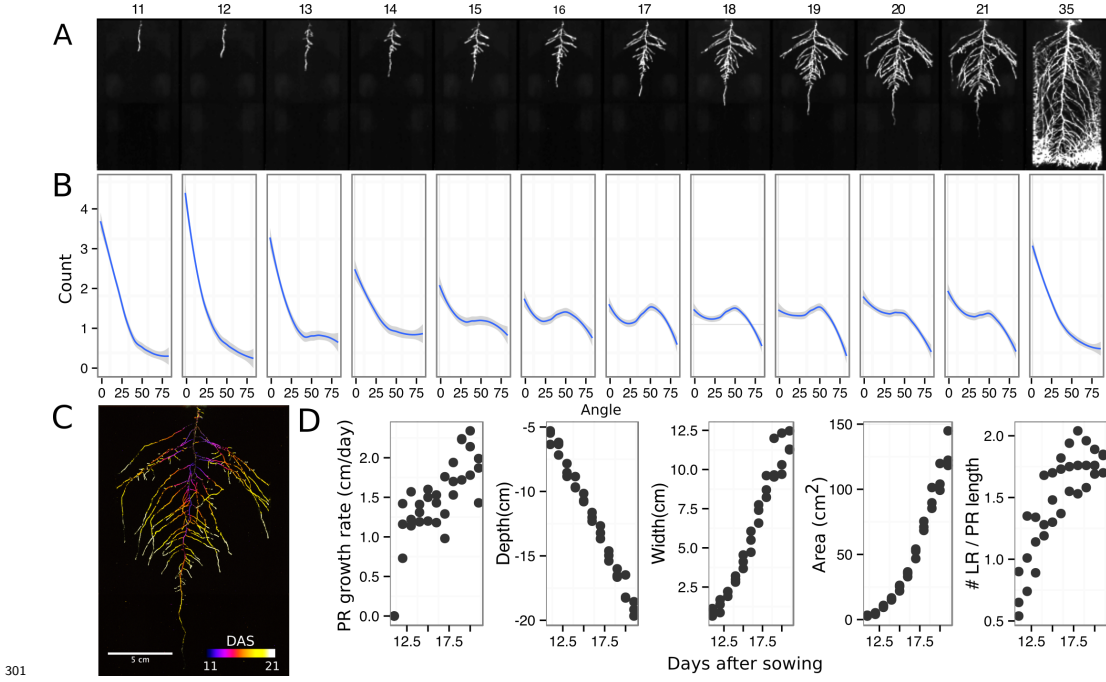
<sup>274</sup> GLO-RIA does not currently have the ability to reconstruct the root architecture in itself  
<sup>275</sup> (topological links between roots). This is a challenge for analyzing images captured by GLO-  
<sup>276</sup> Roots since soil particles cause disruption of root segments.

<sup>277</sup> We tested the accuracy of the measurements obtained from GLO-RIA using two different  
<sup>278</sup> ground-truthed data sets. Manual measurement of root system width, depth and average  
<sup>279</sup> lateral root angle was determined by hand using imageJ from an independent set of images  
<sup>280</sup> corresponding to roots of several Arabidopsis accessions growing in control conditions. We  
<sup>281</sup> also used ArchiSimple<sup>19</sup> to generate 1240 images of root system models with contrasting sizes  
<sup>282</sup> and lateral root angles. Since these images are computationally generated, exact determi-  
<sup>283</sup> nation of root system parameters was possible. For both ground truth data sets, GLO-RIA  
<sup>284</sup> quantification provided measurements that were well correlated for all all three measured

285 parameters (Figure 1-figure supplement 5D-F). Sample images of real and ArchiSimple gen-  
286 erated root images are shown with GLO-RIA-defined directionality color-coding (Figure  
287 1-figure supplement 5G-I).

288 **Continuous imaging of root growth.**

289 The size of our rhizotrons enables undisturbed root system development (before roots reach  
290 the sides or the bottom of the rhizotron) for about 21-23 days for the Col-0 accession  
291 growing under long day conditions (Figure 2); however root traits such as directionality  
292 can be observed through later stages of plant development. See 35 DAS root system and  
293 directionality in Figure 2A-B. An example of a time series spanning 11 to 21 days after  
294 sowing (DAS) of Col-0 roots expressing *ProUBQ10:LUC2o* is shown in Fig 2A and [Video 1](#)  
295 with a color-coded time projection shown in Fig 2C. Directionality analysis (Fig 2B) shows  
296 a progressive change in root system angles from 0° (vertical) to 45° as lateral roots take  
297 over as the predominant root type. Figure 2D shows the evolution over time of several root  
298 traits that can be automatically captured by GLO-RIA (depth, width, area) and others that  
299 were manually quantified (primary root growth rate or number of lateral roots per primary  
300 root).

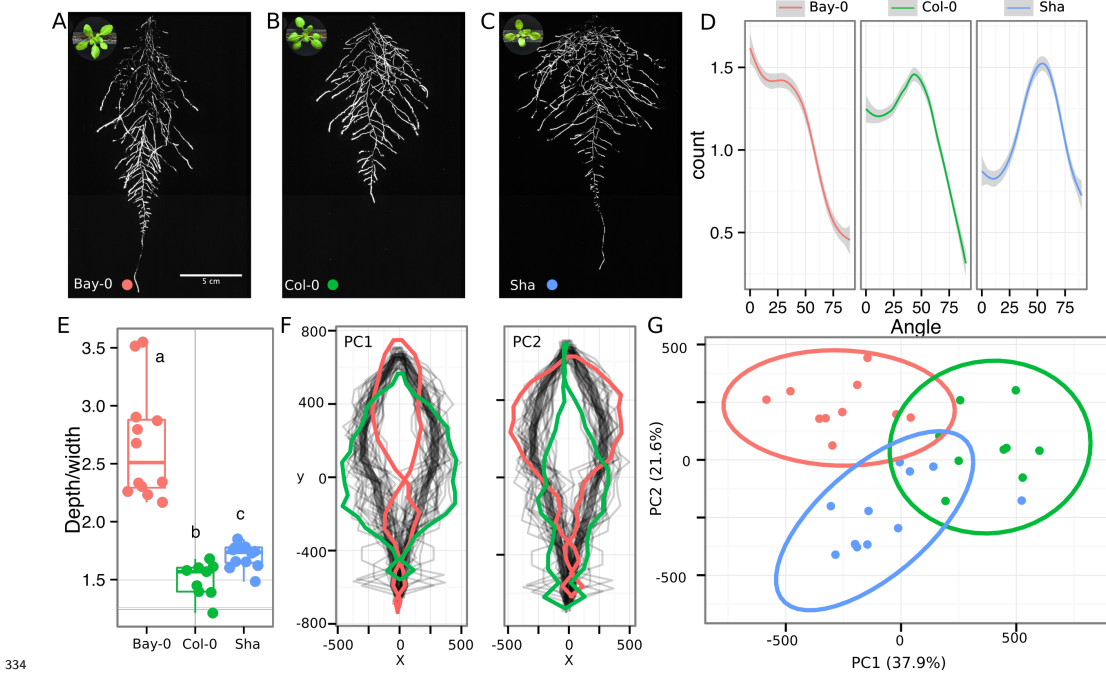


301 **Figure 2. Time-lapse imaging of root systems and quantification using GLO-**  
 302 **RIA.** A) Typical daily time-lapse image series from 11 to 35 DAS of a *ProUBQ10:LUC2o*  
 303 Col-0 plant. B) Directionality of the root system of plants in panel A calculated using the  
 304 directionality plugin implemented in GLO-RIA. C) Color coded projection of root growth  
 305 using the images in panel A. D) Primary root growth rate, depth, width, root system area  
 306 are automatically calculated from the convex hull, which is semi-automatically determined  
 307 with GLO-RIA. Lateral root number and number of lateral roots divided by the primary  
 308 root length were quantified manually. A Local Polynomial Regression Fitting with 95%  
 309 confidence interval (grey) was used to represent the directionality distribution curve. ( $0^\circ$  is  
 310 the direction of the gravity vector).  
 311

312 **Root system architecture of different *Arabidopsis* accessions.**

313 As a proof of concept to estimate the utility of our root imaging system to phenotype  
 314 adult root system traits, we transformed a small set of accessions (Bay-0, Col-0 and Sha)  
 315 with the *ProUBQ10:LUC2o* reporter and quantified RSA at 22 DAS (Fig 3A-C). GLO-RIA

316 analysis of these root systems identified several root traits that distinguish Col-0, Bay-0  
317 and Sha. Directionality analysis revealed an abundance of steep-angle regions in the root  
318 system of Bay while Sha showed an abundance of shallow-angled regions and Col-0 was  
319 intermediate (Fig 3D). Bay-0 shows the deepest and narrowest root system leading to the  
320 highest depth/width ratio while Sha has the widest root system (Fig 3E). Other root traits  
321 such as root system area and the vertical center of mass also showed significant differences  
322 (Figure 3-figure supplement 1B). Broad sense heritability values for depth (96.3), area (92.0),  
323 depth/width (97.8), width (95.7) and vertical center of mass (95.0) were all higher than 90%.  
324 To capture the richness of root architecture shape, we used GLO-RIA to extract pseudo-  
325 landmarks describing the shape of the root system (see Materials and Methods for more  
326 details) and performed PCA analysis. The first principal component captures differences  
327 in the distribution of widths along the vertical axis and separates Col-0 and Sha from Bay-  
328 0 root systems. (Fig 3F). Bay-0 shows an homogenous distribution of widths along the  
329 vertical axis while Sha and Col-0 are much wider at the top than bottom. PC2 seems to be  
330 capturing a relationship between width at the top and total depth and separates Sha root  
331 systems which are wide at the top and deep from Col-0 root systems which are wide but  
332 not as deep as Sha. Shape information extracted from pseudo-landmarks can distinguish  
333 the three different accession using PCA analysis (Fig 3G).



335 **Figure 3. Variation in root architecture between accessions of *Arabidopsis*.** Rep-  
 336 resentative root and shoot images of A) Bay-0, B) Col-0 and C) Sha accessions transformed  
 337 with *\_ProUBQ10:LUC2o\_* and imaged after 22 DAS. D) Directionality of the root systems,  
 338 E) depth/width ratio, F) Pseudo-landmarks describing shape variation in root system archi-  
 339 tecture. Eigenvalues derived from the analysis of 9-12 plants per accession is shown. The  
 340 first two Principal Components explaining 38% (PC1) and 22% (PC2) of the shape variation  
 341 are plotted. PC1 captures homogeneity of root system width along the vertical axis and  
 342 PC2 a combination of depth and width in top parts of the root system. Red and green  
 343 lines indicate -3SD and +3SD (Standard Deviations), respectively G) PC separation of the  
 344 different ecotypes using the PCs described in (F). A Local Polynomial Regression Fitting  
 345 with 95% confidence interval (grey) was used to represent the directionality distribution  
 346 curve. 0° is the direction of the gravity vector. Wilcoxon test analysis with p < 0.01 was  
 347 used to test significant differences between the different accession (n = 9-12 plants).

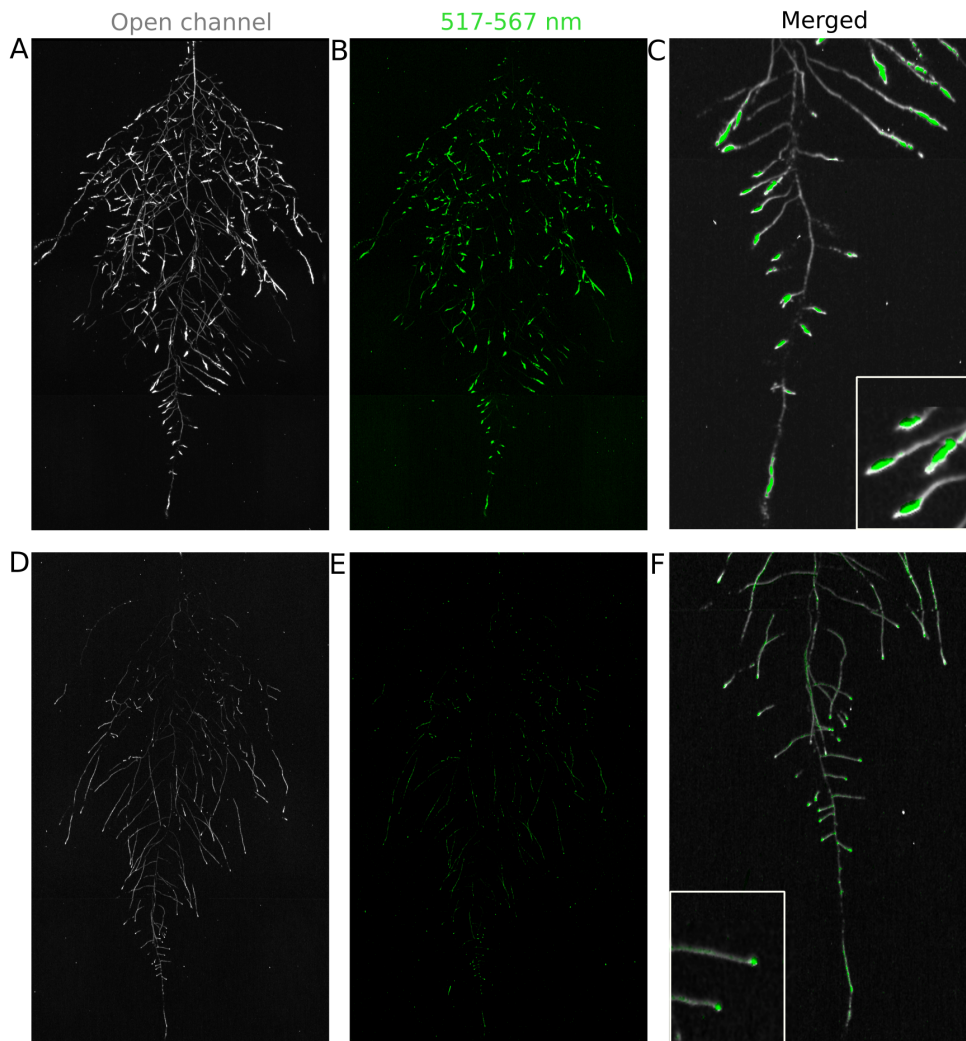
**348 Spectrally distinct luciferases enable gene expression patterns, characterization  
349 of root system interactions and microbial colonization.**

**350** We tested whether spectrally distinct luciferase reporters would enable additional information  
**351** besides root architecture to be captured from root systems. Luciferase reporters have  
**352** been commonly used to study gene expression and these resources can potentially be utilized  
**353** to study such regulatory events in soil-grown roots. We transformed *ProACT2:PpyRE8o*  
**354** into two well studied LUC reporter lines: the auxin response reporter line *ProDR5:LUC*<sup>20</sup>  
**355** (Figure A-B) and the Reactive Oxygen Species (ROS) response reporter *ProZAT12:LUC*<sup>21</sup>  
**356** (Figure 4C-D). We implemented in GLO-RIA an algorithm that semi-automatically identifies  
**357** gene reporter signal and associates this object to the corresponding root structure  
**358** segment. A graphical representation of the results obtained with Root Reporter can be  
**359** observed in Figure 4-figure supplement 1. Reporter intensity values along the first 5 mm of  
**360** root tips can also be observed in Figure 4-figure supplement 2.

**361** We then took advantage of our ability to constitutively express two spectrally different luciferases and imaged the overlapping root systems (one expressing *ProUBQ10:LUC2o* and  
**362** the other *ProACT2:PpyRE8o*). While two root systems were distinguishable using this  
**363** system (Figure 4-figure supplement 3); measurements of root system area did not reveal a  
**364** significant effect on root growth when two plants were grown in the same rhizotron, compared to one; however, further studies are warranted (Figure 4-figure supplement 3).

**367** The GLO-Roots system uses non-sterile growth conditions, which allows complex biotic  
**368** interactions that may affect responses to the environment. Bacteria themselves can be engineered  
**369** to express luminescent reporters through integration of the LUX operon, which results in luminescence in the blue region of the spectrum and is thus compatible with  
**370** the plant-expressed luciferase isoforms we have tested. *Pseudomonas fluorescens* CH267<sup>22</sup>,  
**371** a natural *Arabidopsis* root commensal, was transformed with the bacterial LUX operon  
**372** and used to inoculate plants. Thirteen days after inoculation, we were able to observe  
**373** bacterial luminescence colocalizing with plant roots. *P. fluorescens* did not show an obvious  
**374** pattern of colonization at the root system scale level. As a proof-of-principle test

376 of the multi-dimensional capabilities of the GLO-Roots system we visualized both *LUC2o*  
377 and *PPyRE8o* reporters in plants and the LUX reporter in bacteria in the same rhizotron  
378 (Figure 4-figure supplement 4).



379

380 **Figure 4. Dual-color reporter visualization of structure and gene expression.**

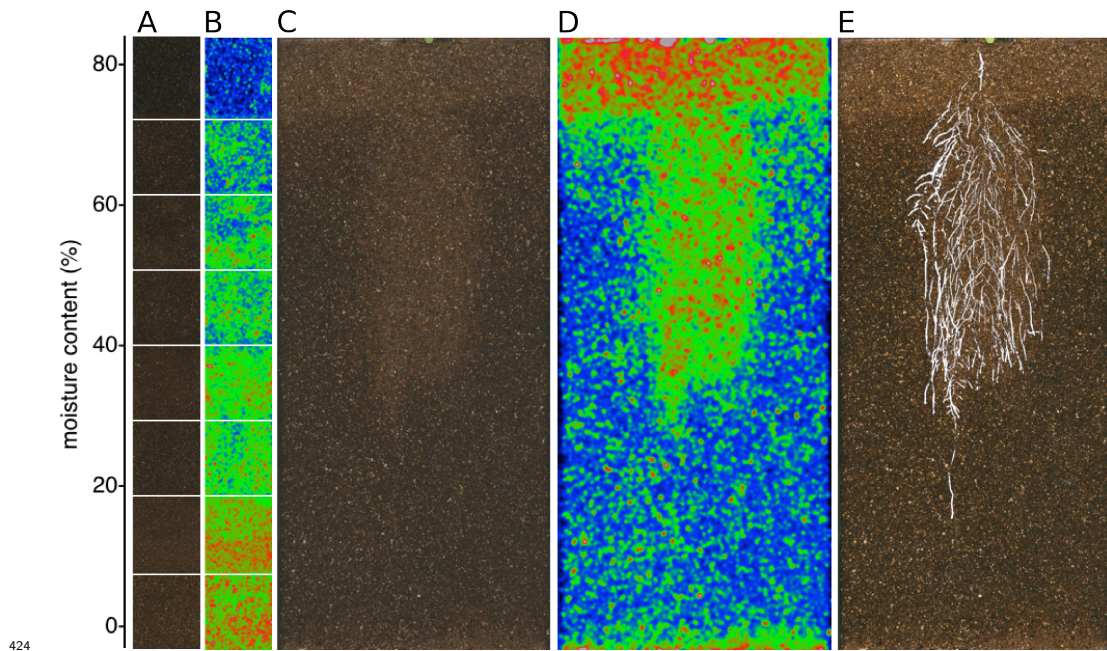
381 Images of whole root systems (A, D) or magnified portion of roots (C, F) at 22 DAS  
382 expressing *ProDR5rev:LUC+* (green, A, B) or *ProZAT12:LUC* signal (green, D, E) with  
383 skeletonized representation of roots generated using the *ProACT2:PpyRE8o* reporter  
384 expression (in grey).

385 **Adaptive changes in root system architecture under water deprivation, phospho-**  
386 **rus deficiency and light.** To test the utility of the GLO-Roots system to understand  
387 response of root systems to environmental stimuli we tested the effects of light and condi-  
388 tions that mimic drought and nutritional deficiency. To examine the effects of light exposure  
389 on the root architecture, the black shields, which normally protect the soil and roots from  
390 light, were removed from the top half of the rhizotrons 10 DAS. Using directionality analysis  
391 we detected a significant increase in the steepness of roots only in the light exposed region of  
392 the rhizotron, while the lower shielded region showed no difference. (Fig 6-figure supplement  
393 3A-B and Fig 6-figure supplement 4). Light can penetrate the top layers of soil<sup>23</sup> and it  
394 has been proposed to have a role in directing root growth specially in dry soils<sup>24</sup> through  
395 the blue light receptor *phot1*. Root directionality was not significantly different between  
396 light and dark-treated roots of the *phot1/2* double mutant suggesting that blue light per-  
397 ception is necessary for this response<sup>24,25</sup> (Fig 6-figure supplement 3B-lower panel). These  
398 data highlight the strong effects of light on root system architecture<sup>26</sup>, which GLO-Roots  
399 rhizotrons are able to mitigate.

400 Plants grown in low-P soil showed a significant increase in the width-depth ratio of the root  
401 system compared to plants grown in P-replete soil, as determined using the automated root  
402 system area finder in GLO-RIA (Fig 6-figure supplement 2A-B). Plants under P deficiency  
403 showed an increase in the ratio between root-shoot area (Fig 6-figure supplement 2C) and  
404 higher investment of resources in the development of the root system at the expense of shoot  
405 growth (Fig 6-figure supplement 2D). Root systems of control and P-deficient plants showed  
406 no significant differences in directionality at 22 DAS but at 27 DAS, roots were more hori-  
407 zontally oriented in P-deficient plants (Fig 6-figure supplement 2E). The observed changes in  
408 root architecture are consistent with root system ideotypes that improve phosphorus uptake  
409 efficiency.

410 GLO-Roots is especially well suited for studying water-deficit (WD) responses. First, shoots  
411 are exposed to the atmosphere and vapor pressure deficit is maintained at levels that allow  
412 for transpiration of water from the shoot. Second, soil in rhizotrons is exposed to air at

413 the top and dries from the top-down; drying soil increases the volume occupied by air and  
 414 reduces contact of root with liquid water, all of which are similar to changes in soil expected  
 415 in the field during WD. Finally, as peat-based soil dries, its optical properties change, al-  
 416 lowing moisture content to be approximated from bright-field images. We took advantage  
 417 of the change in gray-scale pixel intensity to construct a calibration curve (Figure 5-figure  
 418 supplement 1) that quantitatively relates gray-scale pixel intensity to moisture content (Fig  
 419 5A); water content can be color coded in images with appropriate look up tables (Fig 5B).  
 420 Soil color was not affected by the presence or absence of roots (Figure 5-figure supplement  
 421 2). Using this approach, water content in a rhizotron can be mapped and visualized in 2D  
 422 (Fig 5C-D). In the example shown, we can observe that a 22 DAS Bay-0 plant depleted  
 423 soil-moisture content locally around the root system (Figure 5E).

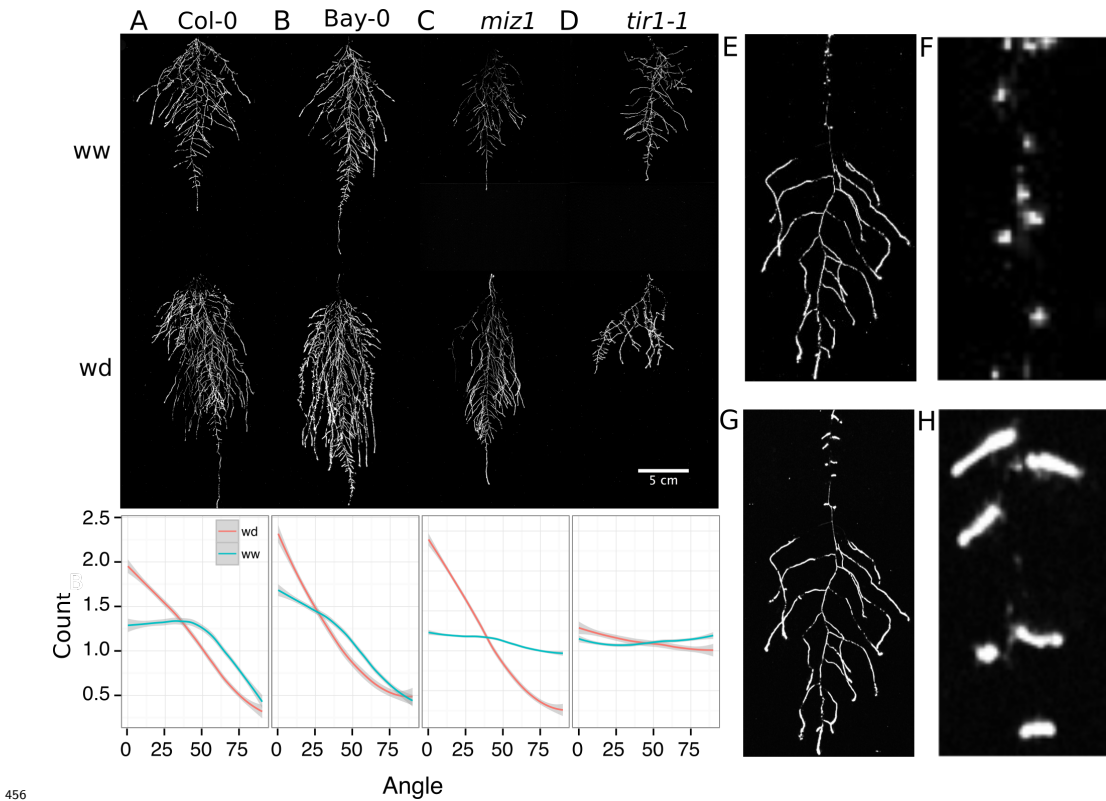


425 **Figure 5. Soil moisture and root architecture mapping in rhizotrons.** A) Com-  
 426 posite image showing regions of soil made from rhizotrons prepared with different moisture  
 427 levels. B) Differences in grey-scale intensity values were enhanced using a 16-color Look  
 428 Up Table (LUT). Brightfield image of soil in rhizotron (C) and converted using 16-color  
 429 LUT to enhance visualization of distribution of moisture (D) . E) Root system of a Bay-0

430 22 DAS and subjected to water deprivation since 13 DAS. Root system visualized using  
431 luminescence and overlaid on brightfield image of soil in (C).

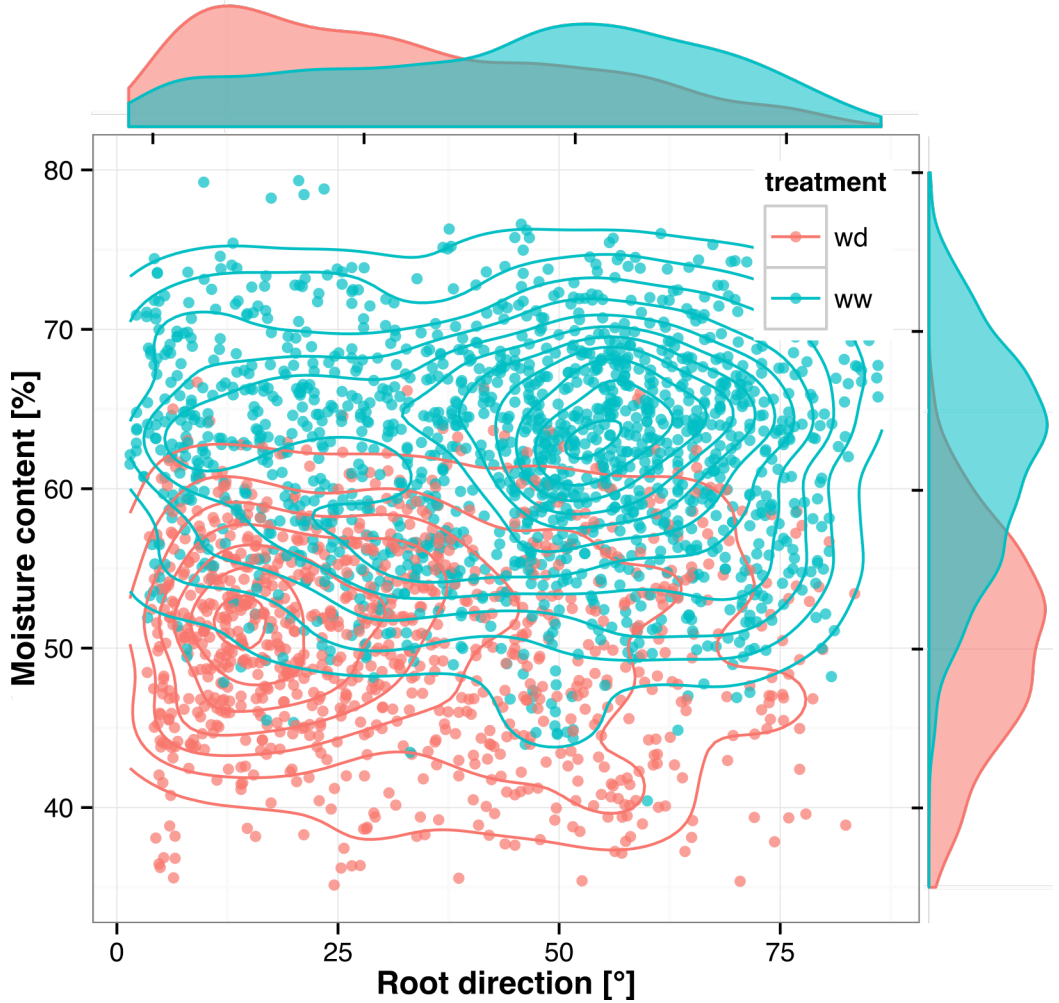
432 We performed several trials to simulate WD in our growth system. Plants were germinated,  
433 grown under control conditions then transferred to 29°C and standing water removed from  
434 the container holding the rhizotrons starting at 9 DAS or 13 DAS. Elevated temperature  
435 combined with water deficit is a common stress that modern crops varieties are poorly  
436 adapted to, thus highlighting the importance of examining this combined treatment<sup>27,28</sup>.  
437 Plants were maintained in this WD regime until 22 DAS when luciferin solution was added  
438 and the plants imaged. At 13 DAS, lateral roots near the soil surface are already emerged  
439 ([Video 1](#), Figure 2A) and 9 days of subsequent WD treatment caused lateral roots to show an  
440 increase in gravitropism leading to the development of a root system that were deeper and  
441 more vertically oriented (Fig 6A). Roots of Bay-0 plants showed similar responses, though  
442 the extent of change was less pronounced since Bay-0 roots are normally more vertically  
443 oriented (Fig 6B). Plants transferred at 9 DAS and grown for 13 days under WD showed  
444 less lateral root development in the top layer of soil (Fig 6E). At this time point, lateral roots  
445 start to emerge ([Video 1](#)) and early drought may lead to growth quiescence or senescence.  
446 Careful examination of roots in these regions showed evidence of small lateral root primordia  
447 populating the primary root (Figure 6F). After 24 h of re-watering (Figure 6G) these lateral  
448 root primordia reinitiated growth (Figure 6H).

449 Time-lapse imaging of the water deficit response showed that changes in root growth direc-  
450 tion occurred ahead of the dry soil front [Video 2](#). Using GLO-RIA we were able correlate  
451 local water moisture contents with the orientation of root segments. With this approach we  
452 observed that root segments in dryer areas of rhizotron grew at steeper root angles (Figure  
453 7) than roots in WW regions, though lateral root angle in wetter regions was also affected.  
454 These data suggest that both local and systemic signaling is likely involved in redirecting  
455 lateral roots deeper during the simulated drought treatments tested here.



456 **Figure 6. Study of effect of water deficit on root system architecture.** A-D)  
457 Root systems 22 DAS and exposed to water deficit 13 DAS onwards. Sample images of  
458 well watered (left panels) and water deficit (right panels) root systems treated from 13  
459 to 22 DAS and directionality (line graphs to left of images) for (A) Col-0 (B) Bay-0 (C) *miz1*  
460 mutant and (D) *tir1-1*. E) Root system of a 22 DAS plant exposed to water deprivation  
461 from 9 DAS onwards with magnified view of lateral root primordia (F). G) The same  
462 root as in (E) 24 hours after rewatering and magnified view of lateral root primordia (H).  
463 Kolmogorov-Smirnov test at  $p < 0.001$  was used to compare directionality distributions  
464 between the different treatments and genotypes. A Local Polynomial Regression Fitting  
465 with 95% confidence interval (grey) was used to represent the directionality distribution  
466 curve.  $0^\circ$  is the direction of the gravity vector.  
467 We also grew plants under WD at control temperatures or under WW conditions at elevated  
468 temperature to test the effects of these individual stresses on root architecture. We observed

470 that both conditions were sufficient to induce a change in root directionality indicating that  
471 the plant uses similar mechanisms to avoid heat and water-deficit associated stresses (Figure  
472 6-figure supplement 1). We next asked which regulatory pathways controlled the observed  
473 changes in lateral root directionality during simulated drought. Hydrotropism is a known  
474 environmental response that directs root growth towards wet regions of soil. MIZ1 is an  
475 essential regulator of hydrotropism; however *miz1* mutants had no significant effect on water  
476 deficit-induced changes in root directionality, compared to wild type (Fig 6C), indicating  
477 that this response was distinct from hydrotropism. Auxin is an important mediator of  
478 gravitropism and auxin treatment causes lateral roots to grow more vertically<sup>7</sup>. Consistent  
479 with this role for auxin, mutant plants with loss of function in the auxin receptor TIR1, did  
480 not show changes in the root system directionality between WW and WD conditions (Fig  
481 6D).



482

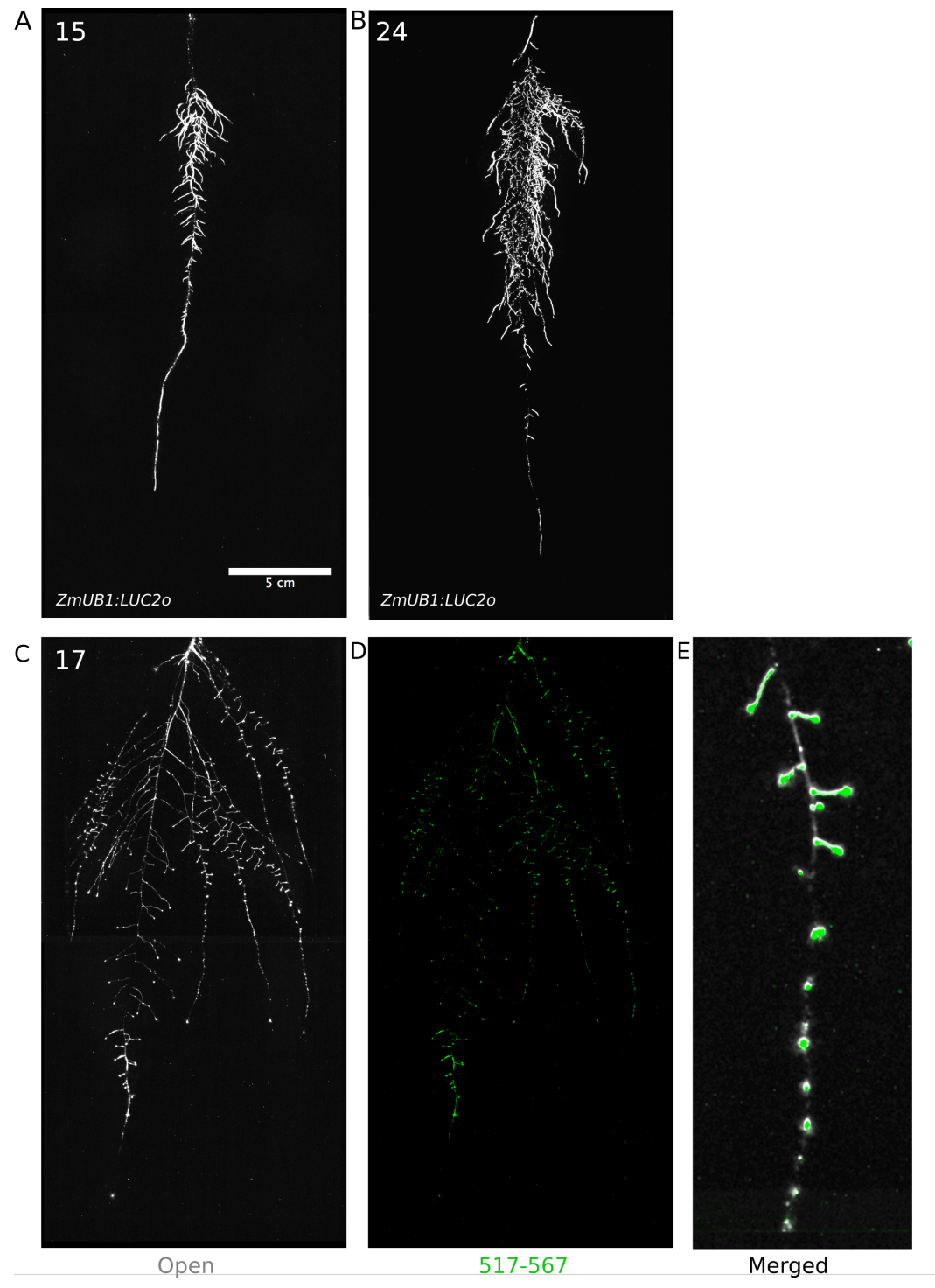
483 **Figure 7. Relationship between local soil moisture content and root growth**  
 484 **direction.** Data quantified from the time lapse series shown in [Video 2](#). Density plots  
 485 shown at periphery of graph for root direction (x-axis) and soil moisture (y-axis).  $0^\circ$  is  
 486 the direction of the gravity vector. Data represents 2535 root tips measured in a series  
 487 encompassing 10 time points.

488 **GLO-Roots for Brachypodium and Tomato.**

489 To examine the general applicability of the GLO-Roots system for other species, we intro-  
 490 duced LUC2o-expressing reporters into the model grass *Brachypodium distachyon* and the

491 crop plant *Lycopersicon esculentum* (tomato). Brachypodium is well suited to the GLO-Root  
492 system because, like Arabidopsis, its small size allows mature root systems to be studied in  
493 relatively small soil volumes<sup>29,30</sup>. *LUC2o* driven by the *ZmUb1* promoter was introduced into  
494 Brachypodium using the pANIC vector<sup>31</sup>. Brachypodium roots showed a distinct architec-  
495 ture from Arabidopsis marked by prolific development of secondary and tertiary lateral roots  
496 (Fig 8A). This is consistent with other studies that show that Brachypodium has a typical  
497 grass root system<sup>30</sup>. Comparison of root system development in rhizotrons with gel-based  
498 media showed that root growth is higher in soil than in plates (Figure 8-figure supplement  
499 1). Previous work has suggested that auxin levels in Brachypodium roots is sub-optimal for  
500 growth<sup>32</sup>. Pacheco-Villalobos and colleagues suggest that, in Brachypodium, and contrary  
501 to what happens in Arabidopsis, ethylene represses *YUCCA* reducing the synthesis of auxin.  
502 The reduced growth that we observe in plates and the high levels of ethylene that build up  
503 in sealed plates<sup>33</sup> would support this mechanism.

504 Tomato plants were transformed with *Pro35S:PPyRE8o* and *ProeDR5rev:LUC2* reporters.  
505 The plants showed more rapid growth than Arabidopsis or Brachypodium and required  
506 fertilizer to prevent obvious signs of stress (reduced growth, anthocyanin accumulation).  
507 Root systems were imaged from 17 DAS plants. Roots showed presumptive lateral root  
508 primordia marked by DR5-expression (Fig 8C-D). These results show that the GLO-Roots  
509 method can be applied to study root systems of plants and will likely be useful for studying  
510 root systems of other small to medium sized model plants and for early stages of larger crop  
511 plants.



512 **Figure 8:** Roots of *Brachypodium distachyon* transformed with *ProZmUB1:LUC2o* and

513

514 imaged at 15 (A) and 24 (B) DAS grown in control conditions. C) Open channel of 17  
515 DAS tomato plant transformed with *ProeDR5rev:LUC2o* and *Pro35S:PPyRE8o* D) Green  
516 channel showing only *ProeDR5rev:LUC2o* E) Amplification of the open and green channel  
517 showing increased expression of *ProeDR5rev:LUC2o* reporter in early-stage lateral roots.

518 **Discussion.**

519 **GLO-Roots enables a multi-dimensional understanding of root biology.**

520 Recent studies of root systems has emphasized structural attributes as important contrib-  
521 utors of root system function. Indeed, studies examining the role of genetic variants in  
522 tolerating abiotic stress have demonstrated the importance of such characteristics<sup>8</sup>. Roots,  
523 however, are highly diverse in the biology they perform and a multi-dimensional understand-  
524 ing of root systems, which incorporates differences in signaling, metabolism and microbial  
525 association as well as structure, may provide a clearer understanding of the degree to which  
526 sub-functionalization of the root system plays a role in important processes such as acclima-  
527 tion and efficient resource acquisition.

528 We have developed tools in GLO-Roots that allow for tracking multiple aspects of soil  
529 physicochemical properties and root biology simultaneously. Using GLO-Roots, we are able  
530 to map in 2D coordinates soil physical properties such soil moisture together with root ar-  
531 chitecture traits such as directionality, growth rates and gene expression levels. All this  
532 information is aggregated in layers for each x, y coordinate. Using GLO-RIA we integrate  
533 this multilayer information, leveraging our ability to simultaneously and seamlessly investi-  
534 gate root responses to environmental stimuli such as soil moisture content. Luciferases that  
535 emit light at different wavelengths allow for constitutive and regulated promoters to be stud-  
536 ied together. Introduction of luciferase reporters into microbes provides an additional layer  
537 of information that provides a readout on the association between organisms and how this  
538 might be affected by environmental conditions. The flexibility of the GLO-Roots system may  
539 enable additional dimensionality to our understanding of root biology. Other physical prop-

540 erties such as CO<sub>2</sub> or pH mapping in rhizotrons have already been enabled by using planar  
541 optodes<sup>34</sup>. It may be possible to engineer LUX-based reporters in microbes that are respon-  
542 sive to extracellular metabolites, creating microbial biosensors, and integration of such tools  
543 may enable root-exudation and nutrition to be analyzed in soil. Split-Luciferase reporters  
544 have been engineered that allow bi-molecular interactions to be studied. Finally, molecular  
545 sensors analogous to FRET sensors, termed BRET-sensors<sup>35</sup>, may allow metabolite tracking  
546 dynamically through the root system. With additional innovation in the development of  
547 luciferase reporters, the GLO-Roots systems will likely expand the repertoire of biological  
548 processes that can be studied over an expanded range of developmental time points and  
549 environmental conditions.

550 **Enhanced root growth and gravitropism may constitute an avoidance mechanism  
551 used during water deficit stress.**

552 It has been proposed that plants with steep root systems will be better able to tap into deep  
553 water resources and thus perform better under water deprivation. For example in rice, the  
554 IR64 paddy cultivar shows shallow root systems in upland fields whereas Kinandang Patong,  
555 an upland cultivar, is deeper rooting<sup>8</sup>. Plants maintain a number of regulatory pathways that  
556 mediate changes in physiology during WD. Enhanced growth of root systems has been well  
557 characterized in field-grown plants; however this has not been recapitulated in studies of gel-  
558 grown Arabidopsis plants. Thus, it has been unclear whether Arabidopsis simply responds  
559 to WD differently. Our results here show that Arabidopsis does indeed maintain a classical  
560 WD response that expands the root system and directs growth downward. Interestingly,  
561 under our stress regime, we did not observe a significant decrease in the relative water  
562 content of shoot tissues (Figure 6-figure supplement 5), suggesting that the changes in root  
563 architecture were sufficient to provide access to deep water and prevent dehydration. Such  
564 changes in root growth are likely regulated through systemic and local signaling that involve  
565 auxin signaling but acts independently of known pathways that control moisture-directed  
566 root growth.

567 **Perspectives and Conclusions.**

568 Understanding plant biology requires a sophisticated understanding of how environmental  
569 stimuli affect the form and function of plants as well as an understanding of how physiological  
570 context informs such responses. Environmental conditions are at least as complex as the  
571 plants they affect. Plant roots are exposed to a variety of environmental signals that change  
572 in time and space at very different scales that are integrated at the whole plant system. It is  
573 an important challenge in biology to develop methods of growing and studying plants that  
574 present such stimuli in a manner that the plant is likely to encounter in nature. After all, the  
575 plants we study have evolved to survive through mechanisms that have been selected, over  
576 evolutionary time, in nature. It will be interesting for future studies to determine how other  
577 environmental stimuli affect root growth using GLO-Roots and whether these responses  
578 differ between accessions of Arabidopsis. Identification of the genetic loci responsible for  
579 phenotypic variation in adult root phenotypes may identify the molecular basis for adaptive  
580 variation that exists in this species and potentially identify loci that are useful for breeding  
581 efforts needed for the next green revolution.

582 **Materials and methods.**

583 **Growth system.**

584 **Rhizotrons and growth system fabrication.** Rhizotrons are composed of two sheets of  
585 1/8" abrasion resistant polycarbonate plastic (Makrolon AR (R)) cut to size using a water  
586 jet (AquaJet LLC, Salem, OR), two acrylic spacers cut using a laser (Stanford Product  
587 Realization Lab), two rubber U-channels cut to strips 30 cm long ([McMaster Carr part](#)  
588 [# 8507K33](#)) and two sheets of black 0.030" thick polypropylene sheets ([McMaster Carr](#)  
589 [part # 1451T21](#)) cut with a straight-edge razor blade. Rhizotron designs were drafted in  
590 Adobe Illustrator (Adobe, San José, CA). The blueprints of all the parts are provided in  
591 Supplement 1. The top edge of each polycarbonate sheet was painted with black 270 Stiletto  
592 nail polish (Revlon, New York, NY).

593 **Boxes and holders.** Rhizotrons are held vertical during plant growth in a custom rack sys-  
594 tem composed of two sheets of 1/4" black acrylic plastic cut with slots for eleven rhizotrons  
595 using a laser, four 3/8" PVC rods ([McMaster Carr part # 98871a041](#)) secured with PVC  
596 nuts ([McMaster Carr part # 94806a031](#)) to hold the acrylic sheets horizontal. The rack is  
597 placed inside a 12" x 12" x 12" black polyethylene tank ([Plastic Mart part # R121212A](#)).

598 **Rhizotron preparation** The procedure to construct a rhizotron with soil is as follows:  
599 Two pieces of polycarbonate plastic are laid flat on a table with the spacers inserted. Using  
600 an electric paint gun, a fine mist of water is applied to the bare polycarbonate sheets. Then,  
601 using a 2 mm sieve (US Standard Sieve Series N° 10) a fine layer of PRO-MIX(r) PGX soil  
602 (Premier Tech, Canada) is applied. Excess soil is discarded by gently tapping the plastic  
603 against the table in a vertical position. Water is sprayed again onto the soil, then a second  
604 layer of Pro-MIX is applied as before. For P deficiency experiments soil supplemented with  
605 1 ml of 100 µM P-Alumina (control) and 0-P-Alumina (P deficient ) was used. To prevent  
606 the soil from falling out of the bottom opening, a 3 x 6 cm piece of nylon mesh is rolled into  
607 a 1 cm wide tube and placed at the bottom side of the rhizotron. The spacers are removed  
608 and replaced by clean spacers. The two faces of the rhizotron are carefully joined together  
609 and two rubber U-channels slipped on to clamp all pieces together. Assembled rhizotrons  
610 are placed into the rack inside the boxes and 500 mL of water is added to the box.

611 **Plant growth** *Arabidopsis thaliana* seeds were stratified for 2 d at 4 °C in Eppendorf tubes  
612 with distilled water. Seeds were suspended in 0.1 % agar and 5 to 10 were sown using  
613 a transfer pipette in the rhizotron. A transparent acrylic sheet was mounted on top of  
614 the box and sealed with tape to ensure high humidity conditions that enable *Arabidopsis*  
615 germination. Three days after sowing, the cover was unsealed to decrease humidity and  
616 allow the seedlings to acclimate to a dryer environment. From 3 days after sowing (DAS)  
617 to the time the first true leaves emerged, it was critical to ensure that the top part of the  
618 rhizotron remained humid for proper germination of the plants. Between three and five DAS  
619 the rhizotrons were thinned leaving only the number plants required for that experiment,  
620 typically one, except for experiments examining root-root interactions. Unless otherwise

621 stated, all the experiments presented here, treatments were started 10 DAS. Plants were  
622 grown under long day conditions (16 h light / 8 h dark) using 20–22 °C (day/night) and  
623 150 µE m<sup>-1</sup> s<sup>-1</sup>. Two types of growth environments were used for experiments. A walk-in  
624 growth chamber with fluorescent lightning and a growth cabinet with white LED lights.  
625 Relative water content measurements were done as previously described<sup>36</sup>

626 **qRT-PCR analysis.**

627 Seeds were surface sterilized as described before<sup>2</sup> and grown in rhizotrons, 100 cm<sup>3</sup> pots, or  
628 on two types of 1% agar (Duchefa) media containing either 1x MS nutrients (Caisson) and 1%  
629 Sucrose, (termed ms media) or ¼x MS nutrients only (termed ms25 media). Both media were  
630 buffered using 0.5 g/L MES and pH was adjusted to 5.7 with KOH. All plants were grown  
631 together in a growth cabinet with LED lights under long day conditions (16h day/8h night).  
632 Root and shoot tissue was collected separately from individual plants at the end of the day  
633 (1 hour before the lights shut off) and at the end of the night (1 hour before lights came on).  
634 Three biological replicates were collected for each condition. RNA was extracted using the  
635 Plant RNA MiniPrepTM kit (ZYMO Research) according to manufacturer's instructions  
636 with on-column DNase treatment (Qiagen). cDNA was made using the iScript Advanced  
637 cDNA Synthesis for RT-qPCR kit (Bio-Rad) from 200 ng of total RNA. qRT-PCR was  
638 performed using a Fluidigm BioMarkTM 96.96 Dynamic Array IFC with the EvaGreen®  
639 (Bio-Rad) fluorescence probe according to the Fluidigm Advanced Development Protocol  
640 number 37. For the analysis, all the reactions with no amplification ( $C_t = 999$ ) were set to  
641 the maximal  $C_t$  for that assay type. The two technical replicates were then averaged and  
642  $dC_t$  values calculated using AT3G07480, AT4G37830, At1g13320 and At1g13440 as reference  
643 internal controls. PCA plots were generated with Devium Web<sup>37</sup> using  $dC_t$  values.  $dCT$   
644 values were calculated as  $dCT = CT_{\text{gene interest}} - \text{mean}(CT_{\text{reference gene}})$ . Primers  
645 used are listed in file Supplement 8.

646 **Biological components.**

647   **Codon optimization of luciferases.** The following luciferases that emit light at different  
648   wavelengths were codon optimized for Arabidopsis (Genscript, Piscataway, NJ): LUC2: a  
649   yellow improved version (Promega, Madison, WI) of the original *Photinus pyralis* (firefly)  
650   LUC.

- 651         • Ppy RE8: a red variant<sup>38</sup> of the *P. pyralis* thermostable variant Ppy RE-TS<sup>39</sup>.
- 652         • CBG99: a green variant (Promega, Madison, WI) from yellow click beetle (*Pyrophorus*  
653         *plagiophthalmus*) luciferases.
- 654         • CBR: a red variant (Promega, Madison, WI) from yellow click beetle.

655   **Non-optimized luciferases.** We also used the following non-optimized luciferases:

- 656         • nanoLUC: a blue luciferase isolated from a deep sea shrimp<sup>14</sup>.
- 657         • venusLUC2: a venus-LUC2 fusion reported to show higher luminescence output than  
658         LUC2<sup>15</sup>.
- 659         • A transposon containing the bacterial luciferase-containing LUX operon was inte-  
660         grated into the *Pseudomonas fluorescens* CH267<sup>22</sup> genome by conjugation with *E.*  
661         *coli* SM10 *pir* containing pUT-EM7-LUX<sup>40</sup> and used to track root microbe coloniza-  
662         tion. For inoculation 9 DAS plants were inoculated with 2 mL of an overnight bacterial  
663         culture resuspended in 10 mM MgSO<sub>4</sub> and diluted to 0.01 OD.

664   **Generation of single-reporter transgenic plants.** We generated transcriptional fu-  
665   sions of all luciferases to constitutive promoters to examine the activity level and emission  
666   spectrum of each isoform. The *attL1-attL2* entry clones containing plant-codon optimized  
667   coding sequence of *LUC2*, *PpyRe8*, *CBG99* and *CBR* were synthesized by Genscript. A  
668   DNA fragment including the *UBQ10* promoter region and first intron was amplified from  
669   Col-0 genomic DNA with primers incorporating the attB1, attB4 combination sites at the 5'

and 3' respectively. The PCR product was then introduced into pDONR™ P4-P1R (Invitrogen) through a classic Gateway BP-reaction. The resulting plasmid, the *attL1-attL2* entry clones with luciferase sequences, an empty *attR2-attL3\** entry clone and the destination vector dpGreenmCherry<sup>2</sup> were used to construct *ProUBQ10:LUC2o*, *ProUBQ10:PpyRE8o*, *ProUBQ10:CBG99o* and *ProUBQ10:CBRo* through Gateway LR reactions. The destination vector *dpGreenmCherry* contains a plasma membrane-localized mCherry coding sequence driven by the 35S promoter and is used as a selectable marker of transformation at the mature seed stage<sup>2</sup>. We used Golden Gate cloning and the destination vectors that we had generated before<sup>16</sup> for the following fusions: *ProUBQ10:nanoLUC2*, *ProUBQ10:venusLUC*, *ProACT2:PpyRE8o*. Briefly, the different components of each construct were PCR amplified with complementary BsaI or SapI cutting sites, mixed with the destination vector in a single tube, digested with either BsaI or SapI, ligated with T4 DNA ligase, then transformed into E. coli Top10 cells and plated on LB antibiotic plates containing X-gal as previously described<sup>16</sup>. Junction sites were confirmed by sequencing. We used pSE7 (Addgene ID #: pGoldenGate-SE7: 47676) as the destination vector of the *ProUBQ10:nanoLUC2*, *ProUBQ10:venusLUC* constructs and pMYC2 (Addgene ID #: pGoldenGate-MCY2: 47679) as the destination vector for *ProACT2:PpyRE8o*. Maps of all the vectors can be found in Supplement 8. *ProUBQ10:LUC2o* was transformed into Col-0, Bay and Sha accessions, the *tir1-1*<sup>41</sup> mutant and the *miz1*<sup>42</sup> T-DNA insertion line (SALK\_126928).

**Brachypodium distachyon.** The Arabidopsis plant-codon optimized Luciferase gene, *LUC2o*, was inserted into the monocot vector pANIC10 via Gateway cloning<sup>31</sup>. *Brachypodium distachyon* plants were transformed using the method of Vogel and Hill<sup>43</sup>.

**Tomato.** The transcriptional fusion *ProeDR5:LUC2* was generated by cloning the *ProeDR5:LUC2* DNA fragment into the pBIB expression vector via restriction sites SalI and Acc65I. The eDR5 promoter is an enhanced version of DR5 containing 13 repeats of the 11-nucleotide core DR5 element<sup>44</sup> and the pBIB expression vector contains an NPTII resistance gene under the control of the NOS promoter for use as a selectable marker during

697 transformation. All tomato transformations were performed by the Ralph M. Parsons  
698 Foundation Plant Transformation Facility (University of California, Davis).

699 **Generation of dual-reporter plants.** To generate dual-reporter plants expressing lu-  
700 ciferase isoforms that emit light with divergent emission spectra we used *ProACT2:PpyRE8o*  
701 as the root structural marker and ZAT12:LUC<sup>21</sup> and DR5:LUC+<sup>20</sup> lines that were trans-  
702 formed with the *ProACT2:PpyRE8o* construct. All constructs were transformed using a  
703 modified floral dip method as described in<sup>2</sup>.

704 To make the dual color tomato plants, the *Pro35S:PpyRE8o* transcriptional fusion was  
705 generated by putting the plant-codon optimized coding sequence described above into the  
706 pMDC32 expression vector through a Gateway LR reaction. The pMDC32 vector con-  
707 tains a hygromycin resistance gene under the control of the 35S promoter for use as a se-  
708 lectable marker during transformation. This construct was transformed into the transgenic  
709 *ProeDR5:LUC2* tomato line.

710 **In vivo emission spectra of plants constitutively expressing luciferase isoforms.**

711 To generate *in vivo* emission spectra of all constitutively expressed luciferases, seeds were  
712 sterilized and sown on MS plates as described before<sup>2</sup>. After 8 days, seedlings were treated  
713 with a 100 µM luciferin solution, incubated at room temperature for 3 hours and imaged  
714 using an IVIS Spectrum imaging system (Perkin Elmer, Waltham , MA) using 20 nm band-  
715 pass emission filters at the following wavelengths (in nm: 490-510, 510-530, 530-550, 550-570,  
716 570-590, 590-610, 610-630, 630-650, 650-670, 670-690, 690-710). Raw images were analyzed  
717 using Fiji and *in vivo* emission spectra were constructed. The full emission spectra of LUX  
718 and nanoLUC could not be constructed since the maximum of these two luciferases is below  
719 the lower band pass filter that were available.

720 **Imaging system.** We designed a custom imaging system (GLO1, Growth and Lumines-  
721 cence Observatory 1) optimized for imaging dual-reporter luciferase expression in our custom  
722 rhizotrons. The design was a joint effort with Bioimaging Solutions (San Diego, CA) who

723 also built the system and wrote the acquisition software that drives all the mechanical parts  
724 of the system. The system is composed by two 2048 x 2048 PIXIS-XB cameras (Princeton  
725 Instruments, Trenton, NJ) mounted on top of each other to capture two fields of view en-  
726 compassing approximately two 15 x 15 cm areas corresponding to the top or bottom of the  
727 rhizotron. The cameras are fitted with a Carl-Zeiss macro lens. A filter wheel with space  
728 for four, 76.2 mm filters is positioned in front of the cameras and controlled by a stepper  
729 motor allowing for automated changing of the filter wheel position. We used two -542/50  
730 and 450/70- custom cut Brightline(R) band-pass filters (Semrock, Rochester, NY). In sin-  
731 gle color imaging mode, the filter wheel is operated without filters. Positioned in front of  
732 the filter wheel is a removable rhizotron holder mounted on a stepper motor. This stepper  
733 motor is also controlled by the GLO-1 software allowing automatic acquisition of images  
734 from both sides of the rhizotron sequentially. The whole imaging system is enclosed in a  
735 light-tight black box with a door that allows loading and un-loading of rhizotrons.

736 **Plant Imaging.** Around 50 mL of 300  $\mu$ M D-luciferin (Biosynth, Itasca, IL) was added  
737 to soil at the top of the rhizotron. In general 5 min exposures were taken per rhizotron, per  
738 side, per channel. For daily imaging experiments, plants were imaged at dawn (+/- 1 hr)  
739 to reduce possible effects on diurnal rhythms of keeping plants in the dark during imaging.  
740 Shoot images were taken using a Nikon D3100 camera.

741 **Image Preparation.** Four individual images are collected: top front, bottom front, top  
742 back and bottom back. Using an automated [ImageJ macro](#), a composite image is generated  
743 as follows: 1)To correct for differences in background values between the two cameras the  
744 mean background value of each image is subtracted from 200; 2) images are rotated and  
745 translated to control for small misalignments between the two cameras; 3) the top and  
746 bottom images of each side are merged; 4) the back image is flipped horizontally; 5) the  
747 front and back images are combined using the maximum values. When dual color images are  
748 acquired this operation is repeated for each channel. The final images produced are 16-bit  
749 depth and 4096 x 2048 pixels. The scale of the images is 138.6 pixels per cm. Considering

750 that an Arabidopsis roots is 100  $\mu\text{m}$  this results in 1.39 pixels across an Arabidopsis root.

751 **GLO-RIA imageJ plug-in.** GLO-RIA uses a combination of existing tools to extract  
752 relevant root architecture features. Directionality is acquired using the [directionality plugin](#)  
753 from ImageJ. After the number of direction bins (we usually use bins of  $2^\circ$ ) is defined by the  
754 user, a 5x5 sobel operator is used to derive the local gradient orientation. This orientation  
755 is then used to build a distribution of directions by assigning the square of the orientation  
756 into the appropriate bin. Instead of representing the total counts at each orientation a  
757 relative value is calculated by dividing the individual values at each bin by the total sum  
758 of the histogram (and multiplying by 100). Similar algorithms have been used to quantify  
759 dynamic changes in the plant cytoskeleton<sup>45</sup>.

760 The Elliptic Fourier Descriptors are aquired using the [Fourier Shape Analysis plugin](#) on con-  
761 vex hull shape of the root system. Elliptic Fourier Descriptors have been used in numerous  
762 studies to analyse variations in shapes, notably in leaves (e.g<sup>46</sup>).

763 The shape analysis is inspired by RootScape<sup>17</sup>. Due to the absence of fixed, recognisable  
764 structures in root system (that are required for the position of true landmarks), pseudo-  
765 landmarks are automatically extracted from the root systems. Shortly, the image is divided  
766 vertically at equidistant positions (with the number defined by the user) and for each of the  
767 image stripes, the minimum and maximum x coordinates are computed. The shape analy-  
768 sis is therefore able to discriminate root system with different vertical root distributions or  
769 global root system orientation (e.g. chemotropism) . The code source for the plugin, manual  
770 and sample images can be found in the [github repository](#) of the project.

771 Statistical analysis was performed in R<sup>48</sup>. The tidyR<sup>49</sup>, dplyr<sup>49</sup>, gridExtra<sup>50</sup>, shapes<sup>51</sup>,  
772 geomorph<sup>52</sup>, ggplot2<sup>53</sup> and cowplot<sup>54</sup> packages were used for data preparation, analysis  
773 and plotting. Final figure preparation was done in [Inkscape](#).

774 **Data availability.** All the scripts and original data used to analyze and produce the  
775 images can be accessed in the Github repository of the project: [github.com/rr-lab/GLO-](https://github.com/rr-lab/GLO-)  
776 Roots. Raw files of all the images used in the paper are available in [Dryad](#).

**777 Acknowledgements.**

778 Work in the lab of JRD was funded by the Carnegie Institution for Science Endowment  
779 and grants from the National Science Foundation (MCB-115795) and Department of En-  
780 ergy, Biological and Environmental Research program (DE-SC0008769). RRA was sup-  
781 ported by a Carnegie Postdoc Fellowship and currently by Conacyt Ciencia Básica Joven  
782 Investigador grant number (CB-2014-01-238101). GL was supported by the Belgian Fonds  
783 de la Recherche Scientifique. JM was funded by the National Science Foundation (IOS-  
784 0820854). CH is funded by MGH Toteston & Fund for Medical Discovery Fellowship grant  
785 2014A051303 and NIH R37 grant GM48707 and NSF grant MCB-0519898 awarded to Fred-  
786 erick Ausubel, and previously by the Gordon and Betty Moore Foundation through Grant  
787 GBMF 2550.01 from the Life Sciences Research Foundation. JV was funded by the Office  
788 of Biological and Environmental Research, Office of Science, US Department of Energy, in-  
789 teragency agreements DE-SC0001526 and DE-AI02-07ER64452. We thank Robert Mittler  
790 and Philip Benfey for providing seeds of ZAT12:LUC and DR5:LUC+ respectively.  
791 We also thank Neil Robbins and members of the Dinneny lab for critical review of the  
792 manuscript and suggestions during the development of the project. We greatly appreciate  
793 Tim Doyle at the Stanford Small Animal Imaging Facility for providing advice in the use of  
794 luciferase-based imaging approaches.

**795 Competing interests.**

796 We do not have any competing interests that we are aware of.

930    **References**

- 931    1.Dinneny, J. R. *et al.* Cell identity mediates the response of *Arabidopsis* roots to abiotic  
932    stress. *Science* **320**, 942–945 (2008).
- 933    2.Duan, L. *et al.* Endodermal ABA Signaling Promotes Lateral Root Quiescence during  
934    Salt Stress in Arabidopsis Seedlings. *Plant Cell* **25**, 324–341 (2013).
- 935    3.Lynch, J. P. & Wojciechowski, T. Opportunities and challenges in the subsoil: pathways  
936    to deeper rooted crops. *J. Exp. Bot.* **66**, 2199–2210 (2015).
- 937    4.Brady, N. C. & Weil, R. R. *Elements of the nature and properties of soils*. (Prentice Hall,  
938    2009).
- 939    5.Bao, Y. *et al.* Plant roots use a patterning mechanism to position lateral root branches  
940    toward available water. *Proc Natl Acad Sci* **111**, 9319–9324 (2014).
- 941    6.Tabata, R. *et al.* Perception of root-derived peptides by shoot LRR-RKs mediates systemic  
942    N-demand signaling. *Science* **346**, 343–346 (2014).
- 943    7.Rosquete, M. R. *et al.* An Auxin Transport Mechanism Restricts Positive Orthogravit-  
944    ropicism in Lateral Roots. *Current Biology* **23**, 817–822 (2013).
- 945    8.Uga, Y. *et al.* Control of root system architecture by DEEPER ROOTING 1 increases  
946    rice yield under drought conditions. *Nat. Genet.* **45**, 1097–1102 (2013).
- 947    9.Postma, J. A. & Lynch, J. P. The optimal lateral root branching density for maize depends  
948    on nitrogen and phosphorus availability. *Plant Physiol.* **166**, 590–602 (2014).
- 949    10.Laliberté, E. *et al.* How does pedogenesis drive plant diversity? *Trends in ecology &*  
950    *evolution* **28**, 331–340 (2013).
- 951    11.Tian, H., De Smet, I. & Ding, Z. Shaping a root system: regulating lateral versus primary  
952    root growth. *Trends in plant science* **19**, 426–431 (2014).
- 953    12.Schneider, C. A., Rasband, W. S. & Eliceiri, K. W. NIH Image to ImageJ: 25 years of  
954    image analysis. *Nature methods* **9**, 671–675 (2012).

- 955 13.Meijon, M., Satbhai, S. B., Tsuchimatsu, T. & Busch, W. Genome-wide association study  
956 using cellular traits identifies a new regulator of root development in. *Nat. Genet.* **46**, 77–81  
957 (2013).
- 958 14.Hall, M. P. *et al.* Engineered Luciferase Reporter from a Deep Sea Shrimp Utilizing a  
959 Novel Imidazopyrazinone Substrate. *ACS chemical biology* **7**, 1848–1857 (2012).
- 960 15.Hara-Miyauchi, C. *et al.* Bioluminescent system for dynamic imaging of cell and animal  
961 behavior. *Biochem. Biophys. Res. Commun.* **419**, 188–193 (2012).
- 962 16.Emami, S., Yee, M.-C. & Dinneny, J. R. A robust family of Golden Gate Agrobacterium  
963 vectors for plant synthetic biology. *Front. Plant Sc.* **4**, 339 (2013).
- 964 17.Ristova, D. *et al.* RootScape: a landmark-based system for rapid screening of root  
965 architecture in Arabidopsis. *Plant Physiology* **161**, 1086–1096 (2013).
- 966 18.Lobet, G. *et al.* Root System Markup Language: toward a unified root architecture  
967 description language. *Plant Physiol.* **167**, 617–627 (2015).
- 968 19.Pagès, L. *et al.* Calibration and evaluation of ArchiSimple, a simple model of root system  
969 architecture. *Ecological Modelling* **290**, 76–84 (2014).
- 970 20.Moreno-Risueno, M. A. *et al.* Oscillating gene expression determines competence for  
971 periodic *Arabidopsis* root branching. *Science* **329**, 1306–1311 (2010).
- 972 21.Miller, G. *et al.* The plant NADPH oxidase RBOHD mediates rapid systemic signaling  
973 in response to diverse stimuli. *Science Signaling* **2**, ra45 (2009).
- 974 22.Haney, C. H., Samuel, B. S., Bush, J. & Ausubel, F. M. Associations with rhizosphere  
975 bacteria can confer an adaptive advantage to plants. *Nature Plants* **1**, 15051 (2015).
- 976 23.Mandoli, D. F., FORD, G. A., WALDRON, L. J., NEMSON, J. A. & Briggs, W. R. Some  
977 spectral properties of several soil types: implications for photomorphogenesis\*. *Plant Cell*  
978 *Environ.* **13**, 287–294 (1990).
- 979 24.Galen, C., Rabenold, J. J. & Liscum, E. Functional ecology of a blue light photoreceptor:  
980 effects of phototropin-1 on root growth enhance drought tolerance in *Arabidopsis thaliana*.

- 981    *New Phytol.* **173**, 91–99 (2007).
- 982    25.Moni, A., Lee, A. Y., Briggs, W. R. & Han, I. S. The blue light receptor Phototropin 1  
983    suppresses lateral root growth by controlling cell elongation. *Plant Biology* 34–40 (2014).
- 984    26.Yokawa, K., Kagenishi, T. & Baluška, F. Root photomorphogenesis in laboratory-  
985    maintained *Arabidopsis* seedlings. *Trends Plant Sci.* **18**, 117–119 (2013).
- 986    27.Lobell, D. B. *et al.* Greater Sensitivity to Drought Accompanies Maize Yield Increase in  
987    the U.S. Midwest. *Science* **344**, 516–519 (2014).
- 988    28.Ort, D. R. & Long, S. P. Limits on Yields in the Corn Belt. *Science* **344**, 484–485 (2014).
- 989    29.Pacheco-Villalobos, D. & Hardtke, C. S. Natural genetic variation of root system archi-  
990    tecture from *Arabidopsis* to *Brachypodium*: towards adaptive value. *Philosophical Trans-  
991    actions of the Royal Society of London B: Biological Sciences* **367**, 1552–1558 (2012).
- 992    30.Watt, M., Schneebeli, K., Dong, P. & Wilson, I. W. The shoot and root growth of  
993    *Brachypodium* and its potential as a model for wheat and other cereal crops. *Functional  
994    Plant Biol.* **36**, 960–969 (2009).
- 995    31.Mann, D. G. J. *et al.* Gateway-compatible vectors for high-throughput gene functional  
996    analysis in switchgrass (*Panicum virgatum* L.) and other monocot species. *Plant Biotechnol.  
997    J.* **10**, 226–236 (2012).
- 998    32.Pacheco-Villalobos, D., Sankar, M., Ljung, K. & Hardtke, C. S. Disturbed Local  
999    Auxin Homeostasis Enhances Cellular Anisotropy and Reveals Alternative Wiring of  
1000    Auxin-ethylene Crosstalk in *Brachypodium distachyon* Seminal Roots. *PLoS Genet* **9**,  
1001    e1003564 (2013).
- 1002    33.Buer, C. S., Wasteneys, G. O. & Masle, J. Ethylene modulates root-wave responses in  
1003    *Arabidopsis*. *Plant Physiology* **132**, 1085–1096 (2003).
- 1004    34.Blossfeld, S., Schreiber, C. M., Liebsch, G., Kuhn, A. J. & Hinsinger, P. Quantitative  
1005    imaging of rhizosphere pH and CO<sub>2</sub> dynamics with planar optodes. *Annals of Botany* **112**,  
1006    267–276 (2013).

- 1007 35.Shaw, S. L. & Ehrhardt, D. W. Smaller, Faster, Brighter: Advances in Optical Imaging  
1008 of Living Plant Cells. *Annu. Rev. Plant Biol.* **64**, 351–375 (2013).
- 1009 36.Barr, H. & Weatherley, P. A re-examination of the relative turgidity technique for esti-  
1010 mating water deficit in leaves. *Aust. J. Biol. Sci* **15**, 413–428 (1962).
- 1011 37.Grapov, D. DeviumWeb: Dynamic Multivariate Data Analysis and Visualization Plat-  
1012 form.
- 1013 38.Branchini, B. R. *et al.* Red-emitting luciferases for bioluminescence reporter and imaging  
1014 applications. *Analytical Biochemistry* **396**, 290–297 (2010).
- 1015 39.Branchini, B. R. *et al.* Thermostable red and green light-producing firefly luciferase  
1016 mutants for bioluminescent reporter applications. *Analytical Biochemistry* **361**, 253–262  
1017 (2007).
- 1018 40.Lane, M. C., Alteri, C. J., Smith, S. N. & Mobley, H. L. T. Expression of flagella is  
1019 coincident with uropathogenic Escherichia coli ascension to the upper urinary tract. *Proc.  
1020 Natl. Acad. Sci. U.S.A.* **104**, 16669–16674 (2007).
- 1021 41.Ruegger, M. *et al.* The TIR1 protein of Arabidopsis functions in auxin response and is  
1022 related to human SKP2 and yeast grr1p. *Genes Dev* **12**, 198–207 (1998).
- 1023 42.Moriwaki, T. *et al.* Hormonal Regulation of Lateral Root Development in Arabidopsis  
1024 Modulated by MIZ1 and Requirement of GNOM Activity for MIZ1 Function. *Plant Physiol.*  
1025 **157**, 1209–1220 (2011).
- 1026 43.Vogel, J. & Hill, T. High-efficiency Agrobacterium-mediated transformation of Brachy-  
1027 podium distachyon inbred line Bd21-3. *Plant Cell Rep* **27**, 471–478 (2008).
- 1028 44.Covington, M. F. & Harmer, S. L. The Circadian Clock Regulates Auxin Signaling and  
1029 Responses in Arabidopsis. *Plos Biol* **5**, e222 (2007).
- 1030 45.Lindeboom, J. J. *et al.* A Mechanism for Reorientation of Cortical Microtubule Arrays  
1031 Driven by Microtubule Severing. *Science* **342**, 1245533–1–1245533–11 (2013).

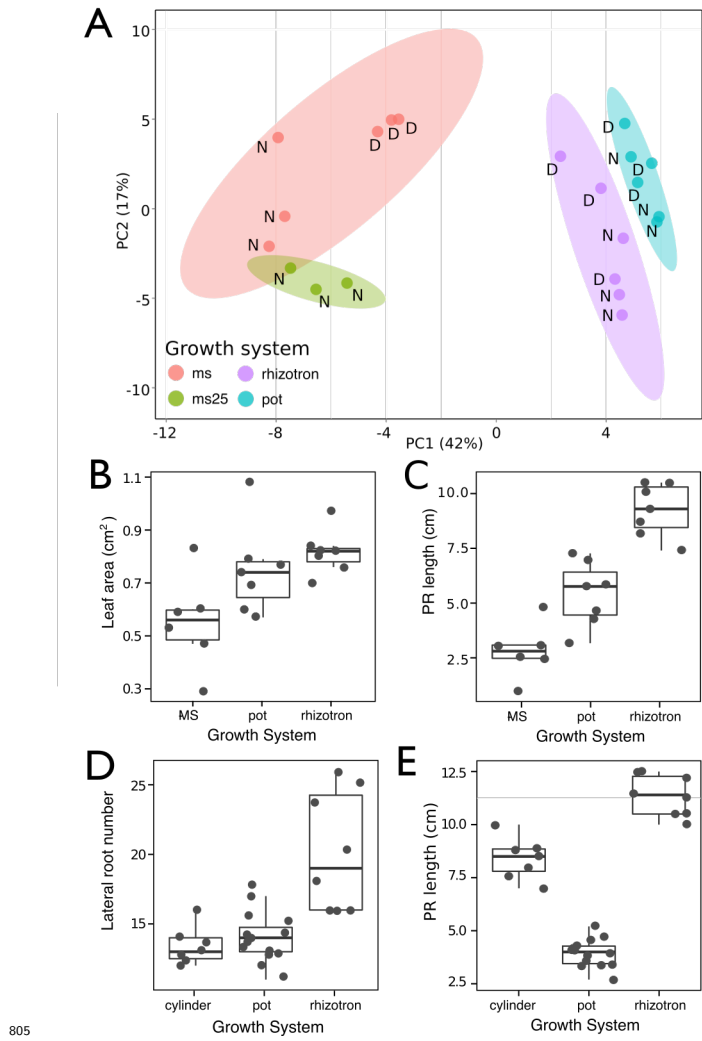
- 1032 46.Chitwood, D. H. *et al.* A modern ampelography: a genetic basis for leaf shape and  
1033 venation patterning in grape. *Plant Physiology* **164**, 259–272 (2014).
- 1034 47.Iwata, H. & Ukai, Y. SHAPE: a computer program package for quantitative evaluation of  
1035 biological shapes based on elliptic Fourier descriptors. *The Journal of Heredity* **93**, 384–385  
1036 (2002).
- 1037 48.R Core Team. *R: A language and environment for statistical computing*. (R Foundation  
1038 for Statistical Computing, 2014). at <<http://www.R-project.org/>>
- 1039 49.Wickham, H. *Tidyr: Easily tidy data with spread() and gather() functions*. (2014). at  
1040 <<http://CRAN.R-project.org/package=tidyr>>
- 1041 50.Auguie, B. *GridExtra: Functions in grid graphics*. (2012). at <<http://CRAN.R-project.org/>>/  
1042 [package=gridExtra](http://CRAN.R-project.org/package=gridExtra)>
- 1043 51.Dryden, I. L. *Shapes: Statistical shape analysis*. (2013). at <<http://CRAN.R-project.org/>>/  
1044 [package=shapes](http://CRAN.R-project.org/package=shapes)>
- 1045 52.Adams, D. & Otarola-Castillo, E. Geomorph: An r package for the collection and analysis  
1046 of geometric morphometric shape data. *Methods in Ecology and Evolution* **4**, 393–399 (2013).
- 1047 53.Wickham, H. *Ggplot2: Elegant graphics for data analysis*. (Springer New York, 2009).  
1048 at <<http://had.co.nz/ggplot2/book>>
- 1049 54.Wilke, C. O. *cowplot: Streamlined Plot Theme and Plot Annotations for ggplot2*. (2015).  
1050 at <<http://cran.r-project.org/web/packages/cowplot/index.html>>

<sub>797</sub> **Videos**

<sub>798</sub> **Video 1** Time lapse from 11 to 21 DAS of a Col-0 plant expressing ProUBQ10:LUC2o  
<sub>799</sub> grown in control conditions

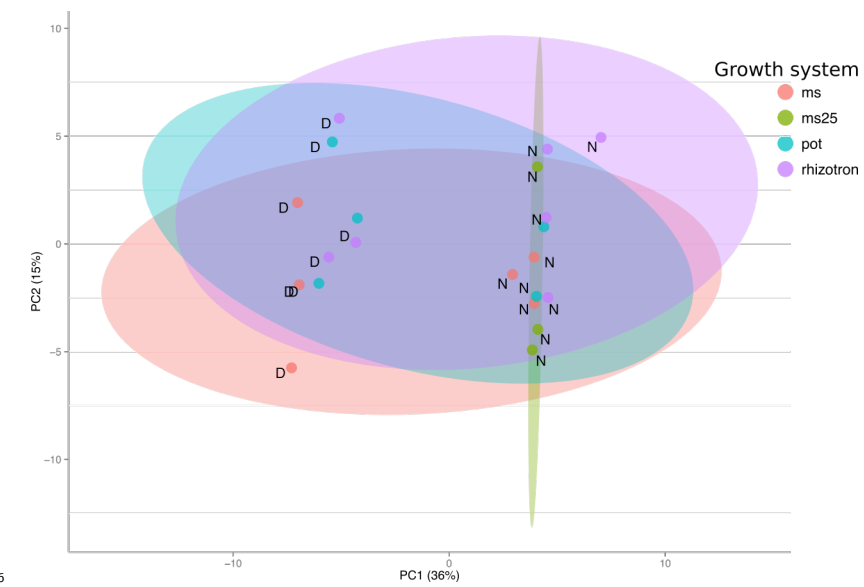
<sub>800</sub> **Video 2** Time lapse from 16 to 24 DAS of Col-0 plants expressing *ProUBQ10:LUC2o*  
<sub>801</sub> growing in water deficient (left) and control (right) conditions. Plants were sown under  
<sub>802</sub> control conditions and water deficit treatment started 11 DAS. Images were taken every  
<sub>803</sub> day.

804 Supplementary figures



805  
806 **Figure 1-figure supplement 1. Effect of different growth systems on plant biol-**  
807 **ogy.** A) Principal Components Analysis (PCA) score plot of a set of 76 genes analyzed by  
808 qPCR from root samples of plants grown in MS plates, pots, and rhizotrons. After 15 DAS  
809 three plants were collected at the end of the day (D) and three were collected at the end of  
810 the night (N). (ms = plant grown in full ms and 1% sucrose, ms25 = plants grown in 25%  
811 of full ms) B) Lateral root number and G) primary root length of 18 DAS plants grown in  
812 30 cm tall cylinders, pots and rhizotrons, all with a volume of 100  $\text{cm}^3$  (n = 6-12 plants).  
813 D) Leaf area and E) primary root length of plants of the same age (15 DAS) as the ones

<sub>814</sub> used for the qPCR experiment (n= 6-7). ANOVA analysis with p < 0.01 was used to test  
<sub>815</sub> significant differences between the different parameters.



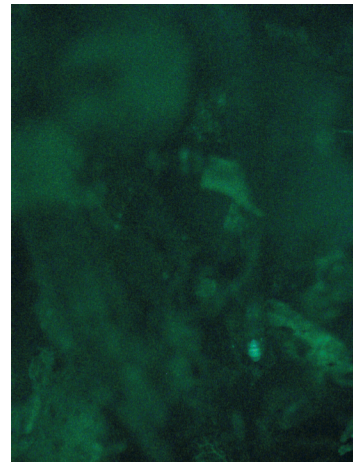
817 \*Figure 1-figure supplement 2. PCA plot of shoots of the same samples analyzed in Figure

818 1. See Figure 1 for more details regarding experimental conditions used.



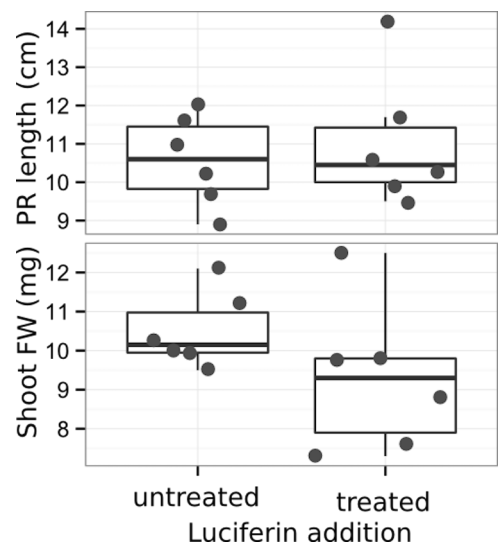
Brightfield

819

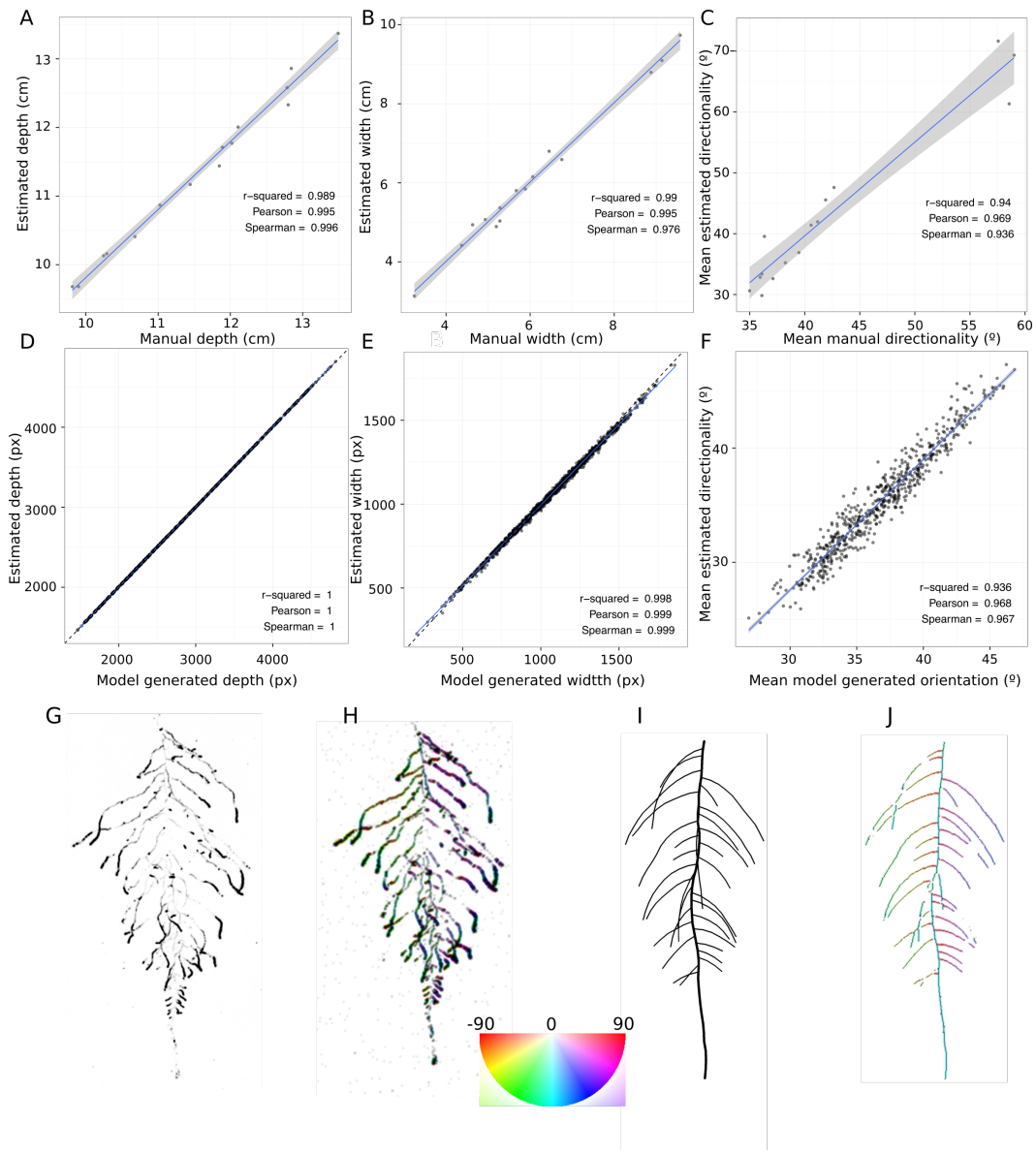


GFP

820 **Figure 1-figure supplement 3** Image of an Arabidopsis root in soil imaged with white  
821 light (brightfield) or epifluorescence.



822     **Figure 1-figure supplement 4** Effect of luciferin addition on primary root length and  
 823     shoot size of 14 DAS seedlings that were either continuously exposed to 300  $\mu$ M luciferin  
 824     from 9 DAS after sowing or not.  
 825



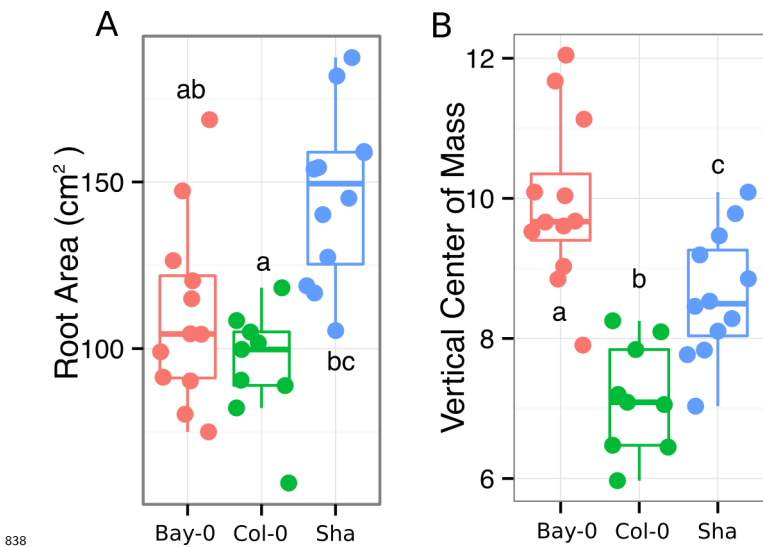
826

827 **Figure 1-figure supplement 5** GLO-RIA ground truth comparison. Tests of GLO-RIA  
 828 were performed using two approaches. We first manually quantified root system depth (A)  
 829 width (B) and average lateral root angle (C) in a set of 15 root systems corresponding  
 830 to different *Arabidopsis* accessions. We also generated 1240 contrasting root systems  
 831 using ArchiSimple and quantified root system depth (D) width (E) and directionality  
 832 (F) using GLO-RIA. Example of a real (G) and ArchiSimple generated (H) root system

<sup>833</sup> and corresponding GLO-RIA determined directionality color-coded into the image (I, J).

<sup>834</sup> Absolute orientation angle values are taken before all calculations.

<sup>835</sup> **Figure 1-figure supplement data 1:** Two way ANOVA P-values comparing plants grown  
<sup>836</sup> in MS media vs. plants grown in soil (pots or rhizotrons) and plants collected at day or night.  
<sup>837</sup> We used p-value < 0.00065 threshold based on Bonferoni adjustment for multiple testing.



839 **Figure 3-figure supplement 1** A) root area, B) vertical center of mass of Bay-0, Col-0  
840 and Sha accessions.

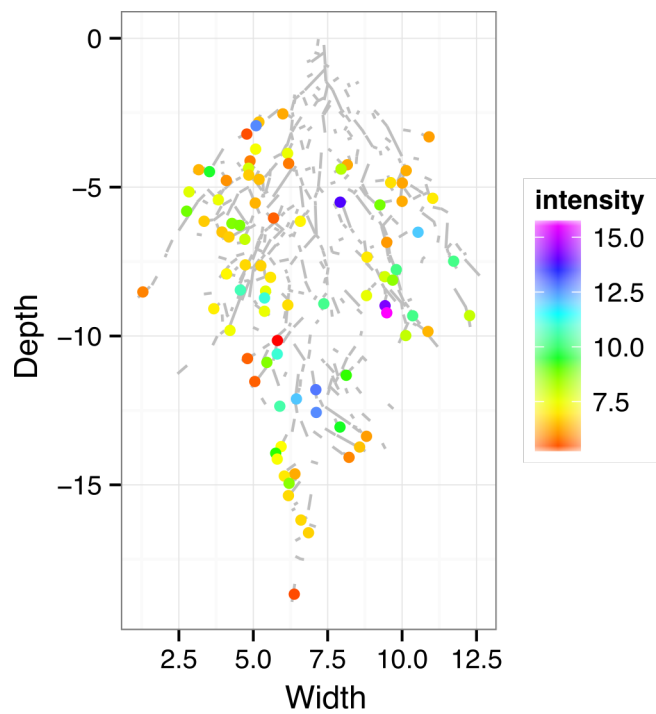
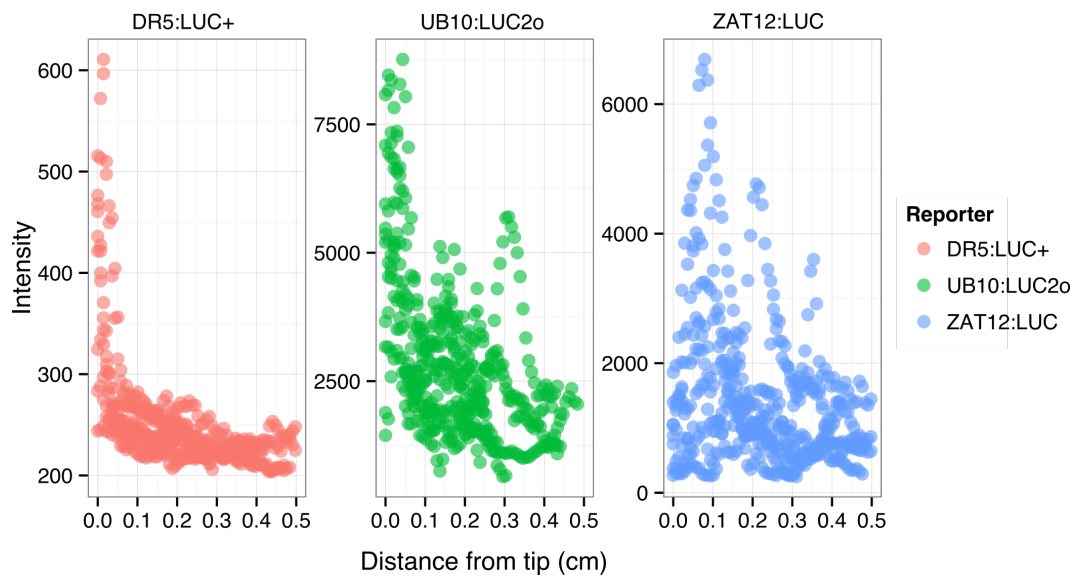


**Figure 4-figure supplement 1:**

841

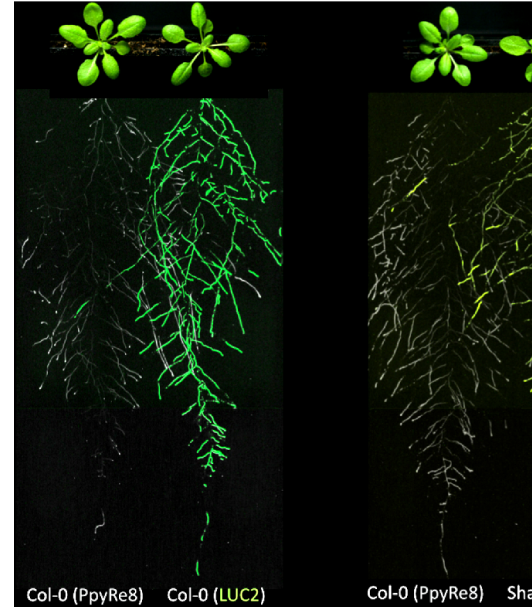
842 ZAT12:LUC intensity and root segments automatically identified with GLO-RIA.



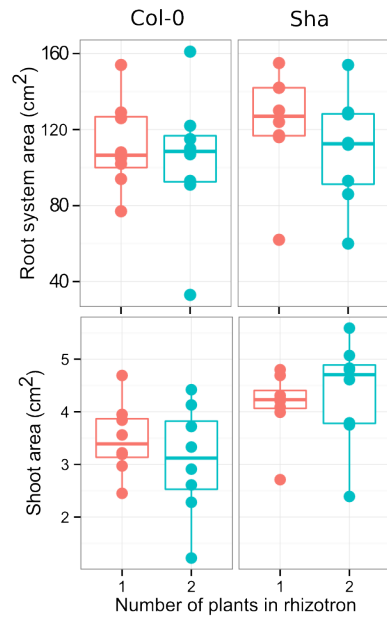
843

844 **Figure 4-figure supplement 2:** DR5:LUC+, UBQ10:LUC2o and ZAT12:LUC intensity  
 845 values along the root tip. Data was manually obtained by obtaining the intensity profile  
 846 of the first 0.5 cm from the root tip of individual lateral roots. Ten lateral roots for each  
 847 reporter were measured.

848

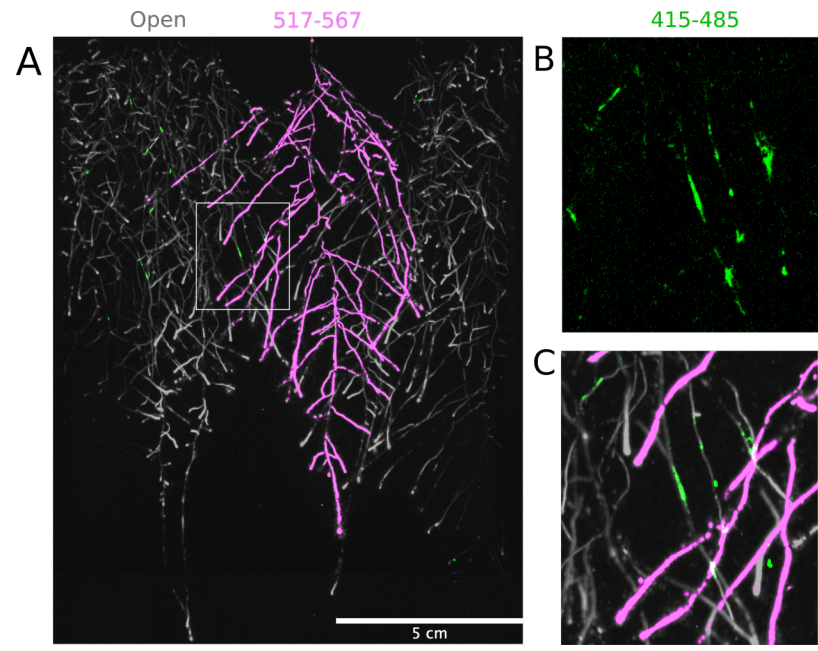


849



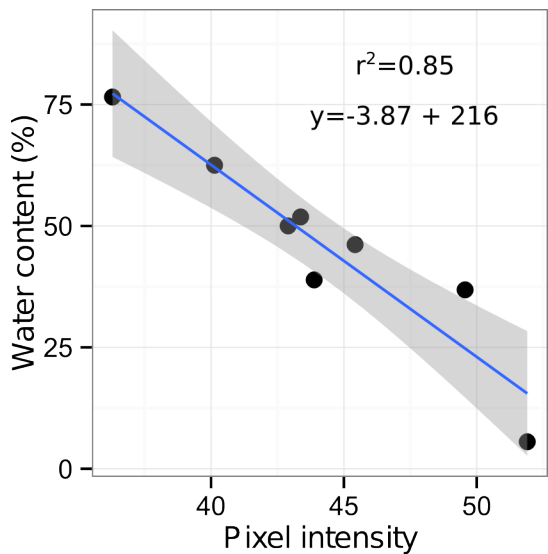
850 **Figure 4-figure supplement 3.** Images of plants at 22 DAS growing in the  
 851 same rhizotron and expressing different luciferases. A) Two Col-0 plants expressing  
 852 *ProUBQ10:LUC2o* and *ProACT2:PPyRE8o* B) Col-0 plant expressing *ProACT2:PPyRE8o*  
 853 and Sha plant expressing *ProUBQ10:LUC2o*.

854



855   **Figure 4-figure supplement 4. Three-reporter-based analysis of root-root-**  
 856   **microbe interactions.** A) Image showing a 22 DAS *ProUBQ10:LUC2o* plant (magenta)  
 857   grown in the same rhizotron with *ProACT2:PpyRE8o* plants (grey). Plants were inoculated  
 858   with *Pseudomonas fluorescens* CH267 (green). Magnified portion of root systems colonized  
 859   by *Pseudomonas fluorescens* showing *P. fluorescences* (B) only or all three reporters  
 860   together (C).

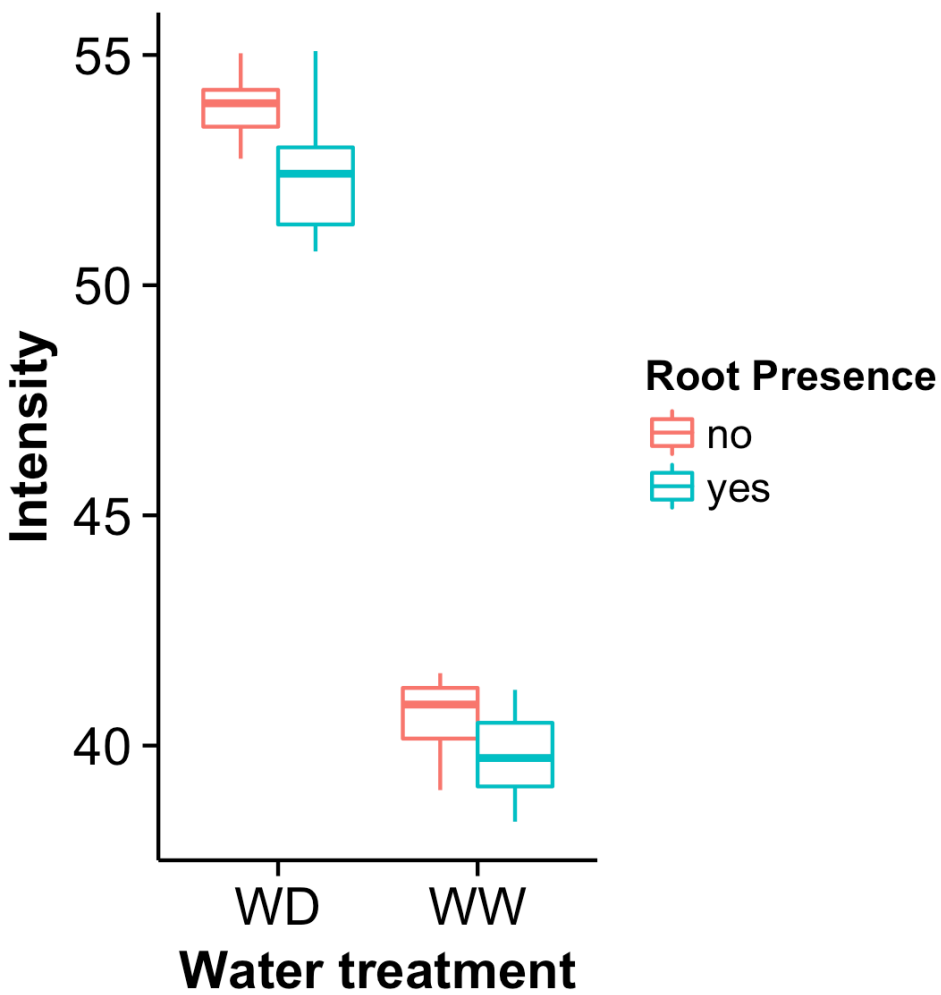
862



863

864 **Figure 5-figure supplement 1:** Moisture calibration curve. Rhizotrons with different  
865 levels of moisture were prepared and scanned to obtain readings of pixel intensity. Soil from  
866 rhizotrons was then weighed, dried down in an oven at 70 °C for 48 hours and percent water  
867 content quantified.

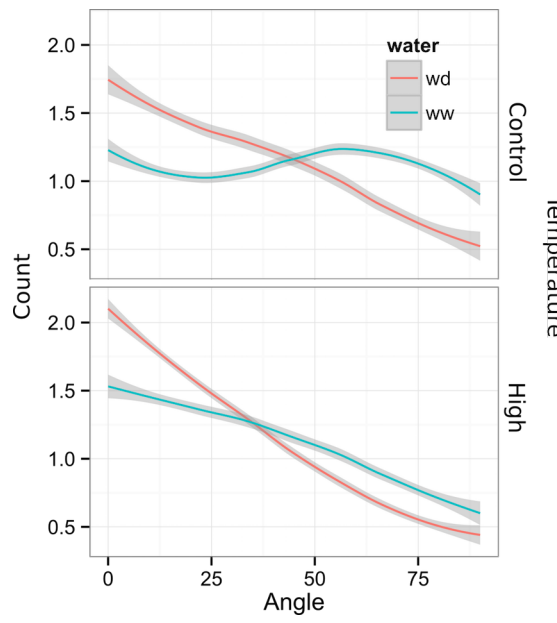
868



869

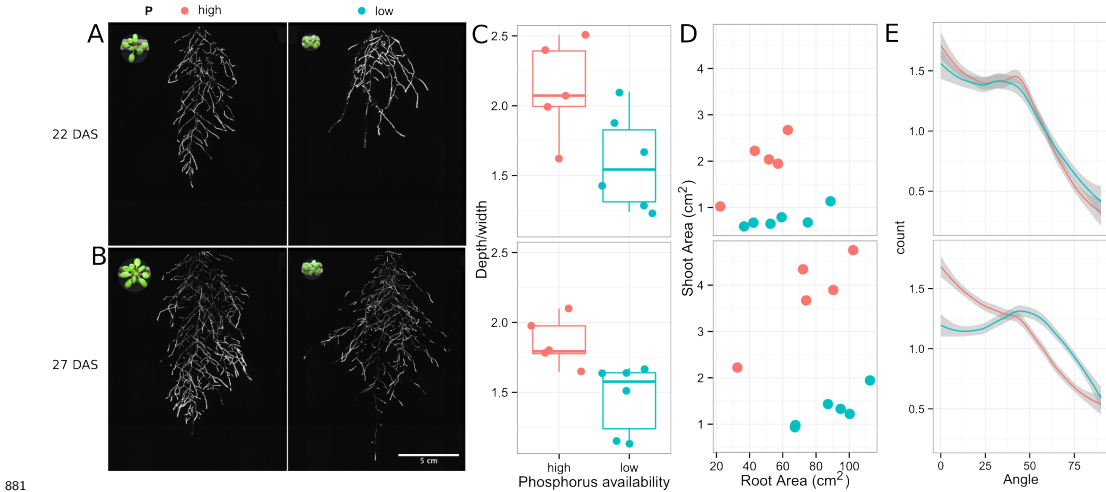
870 **Figure 5-figure supplement 2.** Comparison of soil intensity values between  
871 **areas of the rhizotron with or without the presence of roots, determined based**  
872 **on luminescence data.** Mean intensity values from 100 x 100 pixel squares samples of  
873 both areas were obtained from 10 different rhizotrons. Wilcoxon test analysis with  $p < 0.01$   
874 was used to test significant differences between areas with our without root presence.

875



876  
877 **Figure 6-figure supplement 1** Directionality analysis of roots of plants transferred to  
878 water deprivation conditions after 9 DAS and kept 22 °C (control temperature) and 29 °C  
879 (high temperature) until 22 DAS. (0° is the direction of the gravity vector).

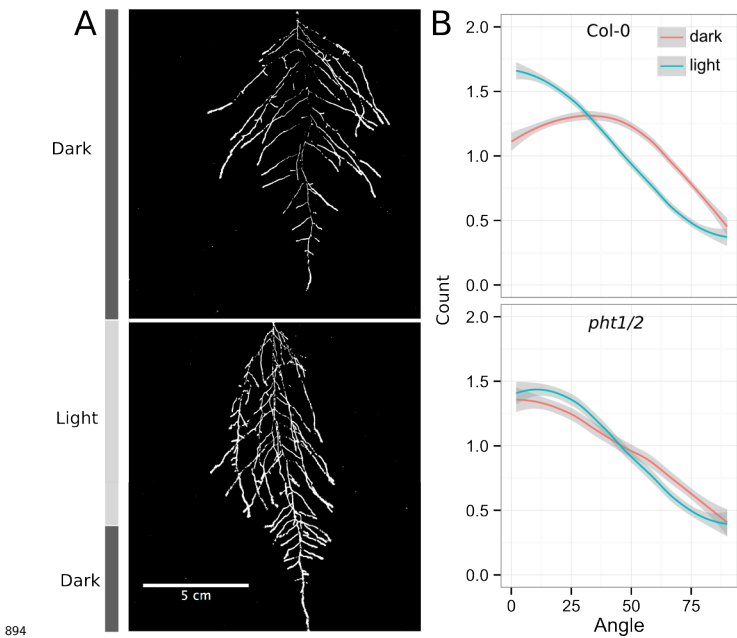
880



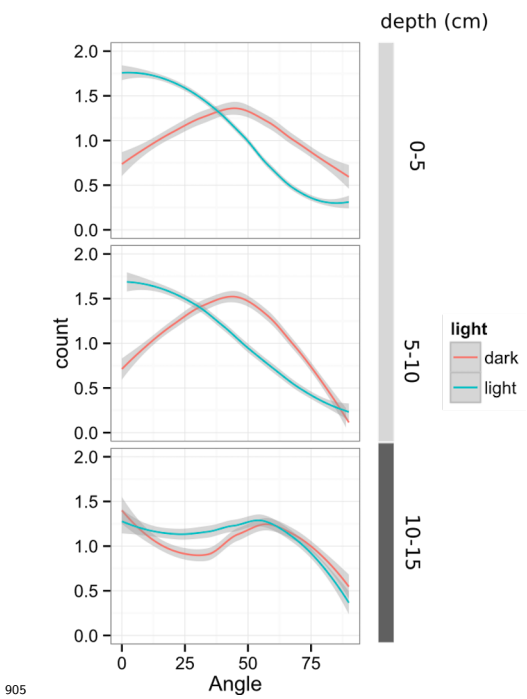
881 **Figure 6-figure supplement 2. Phosphorus deficiency response of root systems**

882 Shoot and root systems of *ProUBQ10:LUC2o* Col-0 plants growing in soil supplemented  
 883 with 1ml of 100  $\mu$ M P-Alumina (left) and 0-P-Alumina (right) 22 (A) or 27 (B) DAS. C)  
 884 Root depth/width ratio of 22 (top) and 27 (bottom) DAS plants. D) Scatter-plot showing  
 885 relationship between root and shoot system area at 22 (top) and 27 (bottom) DAS. E)  
 886 Root directionality distribution in plants 22 (top) and 27 (bottom) DAS. Anova analysis at  
 887 p < 0.01 was used to compare depth/width ratios in P treatments. Kolmogorov-Smirnov  
 888 test at p < 0.001 was used to compare directionality distributions between the different  
 889 treatments. A Local Polynomial Regression Fitting with 95% confidence interval (grey)  
 890 was used to represent the directionality distribution curve.(0° is the direction of the gravity  
 891 vector).

892

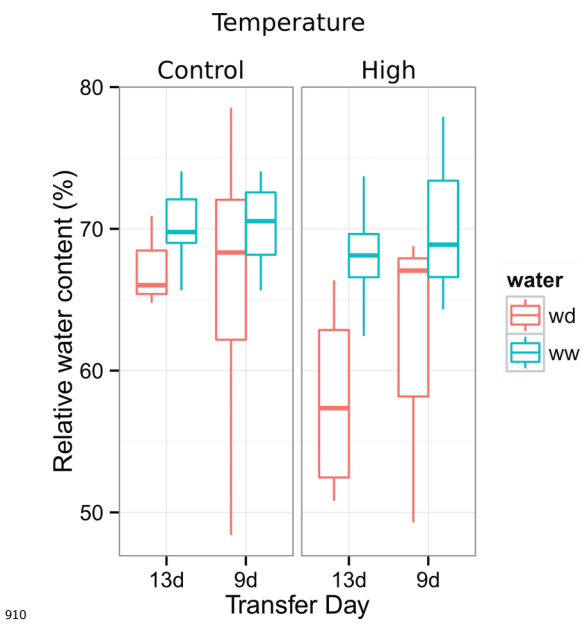


894  
895 **Figure 6-figure supplement 3. Effect of light on root directionality.** A) Col-0  
896 root systems shielded (top) or light exposed (bottom). After 9 DAS the top third of the  
897 rhizotron was exposed to light (indicated on the side with a light grey bar) and plants were  
898 imaged at 20 DAS. B) Directionality analysis of root systems shielded (red) or exposed  
899 (green) to light for Col-0 (top panel) or *pht1/2* double mutant (bottom panel). Between  
900 4 and 6 plants were analyzed per treatment. ANOVA analysis at  $p < 0.01$  was used to  
901 compare depth/width ratios in P treatments. Kolmogorov-Smirnov test at  $p < 0.001$  was  
902 used to compare directionality distributions between the different treatments. A Local  
903 Polynomial Regression Fitting with 95% confidence interval (grey) was used to represent  
904 the directionality distribution curve. ( $0^\circ$  is the direction of the gravity vector).

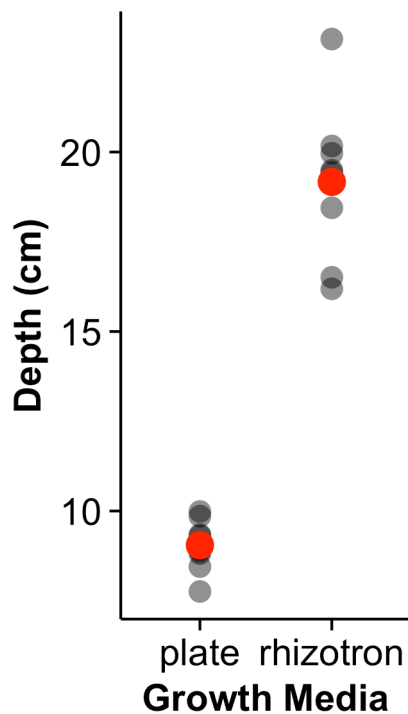


905 **Figure 6-figure supplement 4** Plots showing output of directionality analysis performed  
 906 at different depths (0-5, 5-10, 10-15 cm) in rhizotrons exposed to light or kept in the dark.  
 907  
 908 (0° is the direction of the gravity vector).

909



910     **Figure 6-figure supplement 5.** Leaf relative water content of 23 DAS plants that  
 911     were subjected to water deprivation (WD) after 9 or 13 DAS or kept under  
 912     well watered (WD) conditions. At 9 DAS half of the plants were kept under control  
 913     temperature conditions (22 °C) and the other half transferred to a 29 °C (high) chamber. n  
 914     = 6-8 plants.  
 915  
 916



917

918 **Figure 8-figure supplement 1** Depth of the primary root of *Brachypodium* plants grown  
919 in rhizotrons or on gel-based media (n=8-11). Red dots indicate mean values.

920

921    **Supplementary material**

922    **Supplemental Material 1**

923    Blueprints of the holders, clear sheets and spacers needed to built the rhizotrons. Additional  
924    details are provided in the materials and methods. Files are provided in Adobe Illustrator  
925    .ai and Autocad .dxf formats.

926    **Supplemental Material 2**

927    Primers used in the qPCR experiment.

928    **Supplemental Material 3**

929    Vector maps of all the constructs used in this work.